UNIVERSITY OF TORONTO

Department of Civil Engineering

ISBN 0-7727-7003-4
Publication 79-12

STRESS DETERMINATION AT GREAT DEPTH OF THE GEOTHERMAL WELL ON THE UNIVERSITY OF REGINA CAMPUS

J.-C. ROEGIERS
J.D. McLENNAN

DECEMBER 1979

EPB
Open File
80-7

Energy, Mines and Resources Canada | Énergie, Mines et Ressources Canada

Earth Physics Branch | Direction de la physique du globe

1 Observatory Crescent
Ottawa Canada
K1A 0Y3

1 Place de l'Observatoire
Ottawa Canada
K1A 0Y3

GEOTHERMAL SERVICE OF CANADA

STRESS DETERMINATION AT GREAT DEPTH OF THE GEOTHERMAL WELL ON THE UNIVERSITY OF REGINA CAMPUS

J.-C. Roegiers and J.D. McLennan,
Dept. of Civil Engineering,
University of Toronto,
Toronto, Ontario

Contract OSU79-00109
Supply and Services Canada, 1980

110 pages
Price/Prix $30.75

Earth Physics Branch Open File Number 80-7
Ottawa, Canada 1980

ABSTRACT

Hydraulic fracturing of the water source well for the Geothermal Feasibility Project on the campus of the University of Regina was performed during May and June 1979. The field programme and ancillary laboratory experimentation allowed determination of the magnitude and orientation of the in situ principal stresses.

The borehole in which measurements were made was 2215 metres in depth and was drilled on the campus of the University of Regina, Regina, Saskatchewan. The upper 2034 metres of the hole were cased, having an inside diameter of 7 inches (0.179 metres). The lower 175 metres were uncased, with a diameter of 0.222 metres.

Four intervals were successfully fractured, between a depth of 2062 and 2215 metres. It would appear that the Deadwood sandstone may be a zone of transition from a state of stress in the Winnipeg where $\sigma_v > \sigma$ HMAX $\tilde{>} \sigma$ HMIN to a situation in the upper part of the Precambrian where σ HMAX is slightly greater than the vertical stress.

RESUME

Aux mois de mai et juin 1979, la fracturation hydraulique du puits d'extraction de l'eau pour le Projet de faisabilité géothermique sur le campus de l'Université de Régina fut exécutée. Le programme sur le terrain et l'expérimentation accessoire en laboratoire ont permis la détermination de la grandeur et de l'orientation des tensions in situ principales.

Le forage dans lequel les mesures ont été faites était d'une profondeur de 2215 mètres et situé sur le campus de l'Université de Régina, Régina, Saskatchewan. Les premiers 2034 mètres du trou furent tubés, avec un diamètre intérieur de 7 pouces (0.179 mètres). Les derniers 175 mètres furent non tubés, avec un diamètre de 0.222 mètre.

Quatre intervalles furent fracturés avec succès, entre une profondeur allant de 2062 à 2215 mètres. Il semble que le grès de Deadwood pourrait être une zone de transition entre en état de tension dans le Winnipeg où $\sigma_v > \sigma$ HMAX $\tilde{>} \sigma$ HMIN et un état dans la partie supérieure du Précambrien où σ HMAX est quelque peu plus grand que la tension verticale.

STRESS DETERMINATION AT GREAT DEPTH OF THE GEOTHERMAL WELL ON THE UNIVERSITY OF REGINA CAMPUS

A report, prepared by:

J.-C. Roegiers and J.D. McLennan
Department of Civil Engineering
University of Toronto
35 St. George Street
Toronto, Ontario. M5S 1A4

for

The Department of Supply and Services
(Energy, Mines and Resources)
Contract number: 03SU. 23235-9-0563
0SU79-00109

December 1979

Scientific Authority:

Dr. A.M. Jessop,
Department of Energy, Mines and Resources,
Division of Seismology & Geothermal Studies,
Earth Physics Branch,
1 Observatory Crescent,
Ottawa, Ontario.
K1A 0Y3.

Science Procurement Manager

Mrs. Anita Roodman,
Science Procurement Branch,
Department of Supply and Services,
11C1 Place du Portage - Phase III,
11 Laurier Street,
HULL, Quebec.
K1A 0S5.

ACKNOWLEDGEMENTS

The authors wish to express their gratitude to Dr. A.M. Jessop, Scientific Authority and field representative for the Earth Physics Branch of Energy, Mines and Resources, Canada, and to Dr. L. Vigrass, Director of the Energy Research Unit, University of Regina.

Supervision of the service rig and organization of numerous auxillary services on site was proficiently handled by Mr. D. Rouse.

Additional acknowledgement is due B. Hill and K. Holder of Dikor Services, the members of Halliburton Services and Badge Services.

Particular commendation is due D. Bartolini, W.F. Bawden, and T. Wiles of the Department of Civil Engineering, University of Toronto, for their capable assistance during the field operations and laboratory testing.

SUMMARY

(1) ORIENTATIONS

The measured direction of the maximum *in situ* horizontal principal stress was approximately E-W.

(2) MAGNITUDES OF THE PRINCIPAL STRESS

As vertical fractures were created, the vertical stress was estimated from the weight of overlying material. This is consistent with stress measurements at other localities.

It would appear that the Deadwood sandstone may be a zone of transition from a state of stress in the Winnipeg where $\sigma_V > \sigma_{HMAX} \approx \sigma_{HMIN}$ to a situation in the upper part of the Precambrian where σ_{HMAX} is slightly greater than the vertical stress. The gradient of σ_{HMIN} is approximately constant with depth ($\sigma_{HMIN} \approx .58\ \sigma_V$).

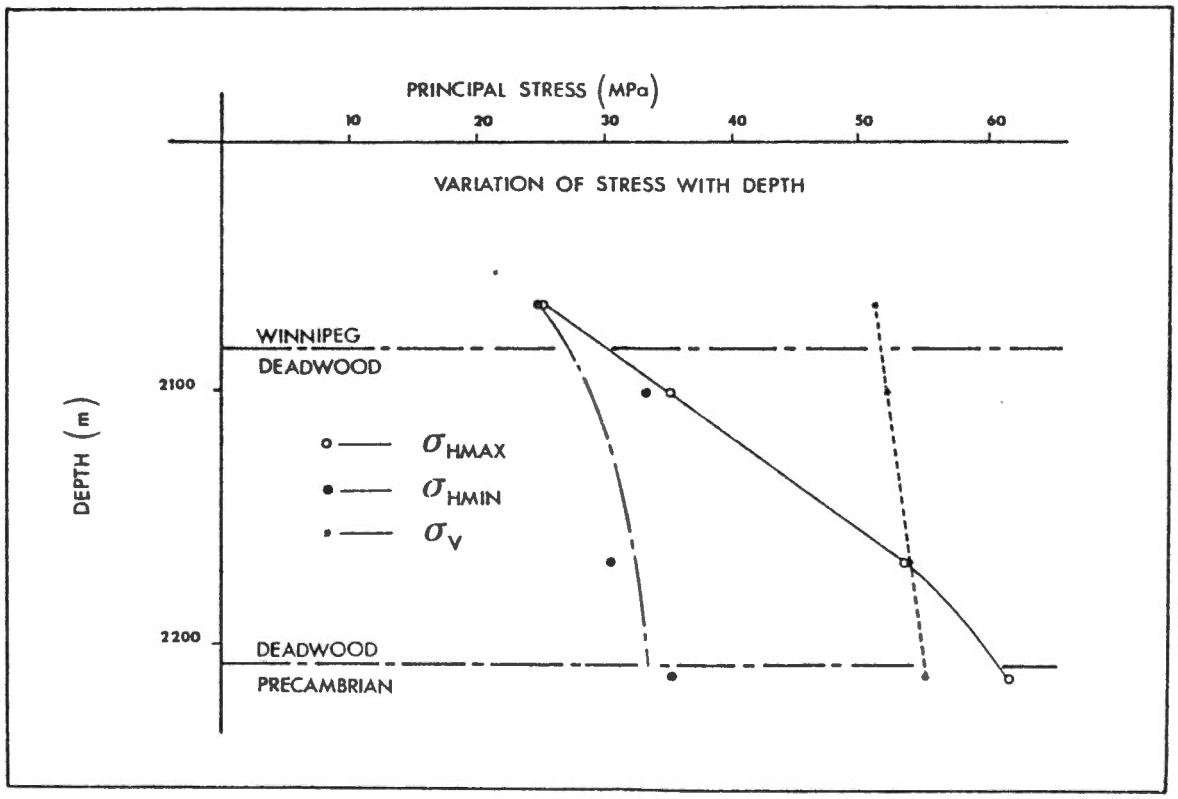

(3) LIMITATIONS OF THE MEASUREMENTS

(i) Only a limited number of measurements were possible.

(ii) As a viscous gel was required to prevent excessive penetration into the formation, fracture propagation after initial breakdown was stable. Consequently, the difference in successive breakdowns could not be used to ascertain tensile strengths. As a result apparent hydraulic fracturing tensile strengths had to be measured using laboratory simulations. Unfortunately, the poorly consolidated nature of many of the sandstones rendered some of the samples not amenable to sample preparation for laboratory testing.

(iii) In one case, breakdown did not immediately occur and may indicate some penetration and consequent pore pressure buildup.

(iv) In some cases, the presence of a mud cake may have led to anomalous breakdown pressures.

TABLE OF CONTENTS

LIST OF TABLES

I. INTRODUCTION

Hydraulic fracturing of the water source well*[1] for the Geothermal Feasibility Project on the campus of the University of Regina was performed during May and June 1979. The field programme and ancillary laboratory experimentation allowed determination of the magnitude and orientation of the *in situ* principal stresses.

The borehole in which measurements were made was 2215 metres in depth and was drilled on the campus of the University of Regina, Regina, Saskatchewan. The upper 2034 metres of the hole were cased, having an inside diameter of 7 inches (0.179 metres). The lower 175 metres were uncased, with a diameter of 0.222 metres.

Four intervals were successfully fractured, between a depth of 2062 and 2215 metres.

The hole inclination was very near to vertical. The horizons fractured were selected in order to:

(i) Provide an adequate representation of the variation of stresses and orientations with depth.

(ii) Induce fractures at depths where pre-existing discontinuities did not exist.

---

*[1] University of Regina 3-8-17-19 well (W. 2nd. Mer.)

II. STRATIGRAPHY

The stratigraphy of the uncased portion of the borehole is represented in Table 1.

TABLE 1

STRATIGRAPHY OF UNCASED SECTION

DEPTH (m)	FORMATION	DESCRIPTION*[1]
2034-2045	Winnipeg Shale (Ordovician)	Grayish green, fissile, waxy claytones with thin interlayered quartzose sandstones
2045-2083	Winnipeg Sandstone (Ordovician)	Quartzose sandstone, characteristically fine to medium-grained with rare coarse grains. Commonly interlayed with thin varicoloured and mottled silty claystones. Often quite friable
2083-2209	Deadwood (Cambrian)	Upper part of the formation is claystones interbedded with quartzose sandstones with argillaceous matrix and potassium bearing accessory minerals (~61 m) Lower part has considerably less claystone and is dominated by semi-consolidated, medium to coarse sandstone.
2209-2215 T.D.=2215	Basement (Precambrian)	Coarse grained, biotite rich granite.

*1 From Vigrass, L.W., Final Well Report, U. of Regina 3-8-17-19, Energy Research Unit, University of Regina, Contribution No. 14.

Table 2 describes the stratigraphy of fractured intervals in a more specific context.

TABLE 2

STRATIGRAPHY OF FRACTURED HORIZONS

FRACTURE NUMBER	DEPTH OF FRACTURE INTERVAL (m)	STRATIGRAPHIC DESCRIPTION
1*	2211-2215 (Precambrian)	Coarse grained biotite rich granite
2*	2165-2170	Kaolin matrix, fine grained white sandstone with minor coarse grains, poor porosity
3*	2062-2067	Sandstone, medium to fine grained with kaolin matrix, often friable, fair to very good porosity, occassional shaley laminae and pyritic stringers
4	2069-2074	As above
5*	2097-2102	2097-2099 - Sandstone-quartz, light grey, fine to medium grained, well cemented, poor porosity, thin filter cake on surface of best porosity. Argillaceous stringers and thin bands of argillaceous, sandy siltstone, tight, pyrite crystals common in argillaceous portions. 2099-2101 - Sandstone - medium grained, fairly well cemented, tight in bands about 8 cm thick. 2101-2102 - Quartz Sandstone - medium grained, occasionally coarse, fairly friable, good porosity, very little argillaceous material, minor (15%) well cemented.

* Indicates *successful hydrofracture*, defined as a test which provides sufficient data to compute both magnitude and orientation of the stress tensor.

III. HYDRAULIC FRACTURING AS A TECHNIQUE FOR STRESS DETERMINATION: AN OVERVIEW

3.1 CLASSICAL APPROACH

Conceptually, hydraulic fracturing involves pressurization of a sealed-off interval in a borehole until rupture of the rock formation, at the pressurized horizon, occurs. The pressure at which this rupture occurs is known as the *breakdown pressure* P_b. After "breakdown", further pumping propagates the fracture away from the borehole wall in a controlled manner. If pumping is discontinued, with the hydraulic circuit maintained closed, an instantaneous *shut-in pressure* is recorded. From equilibrium considerations prevailing at that time, this pressure is approximately equal or slightly above the pressure necessary to keep the fracture open. The two characteristic parameters, breakdown pressure P_b and instantaneous shut-in pressure P_{isip}, are related to the pre-existing stress field provided certain assumptions are made:

(i) Linear elasticity and isotropic conditions prevail.(*)

(ii) The borehole axis is parallel to the one of the principal stresses.

(*) It should be pointed out, however, that the conventional interpretation of hydraulic fracturing data does not require the knowledge of any elastic rock mass parameters; and as such, anisotropic conditions are not incorporated in the interpretation other than by influencing anisotropy in the apparent tensile strength.

The two limiting situations are that:

(i) The vertical stress (σ_v) - or overburden stress - is the least principal stress component.

(ii) The vertical stress (σ_v) is either the intermediate or the largest principal stress.

(i) Vertical Stress as the Maximum or Intermediate Principal Stress

In this case, occurring usually at depths in excess of 1000 feet (300 metres), the shut-in pressure (P_{isip}) is taken equal to the in-situ compressive stress component acting perpendicular to the fracture plane. Provided leakage into the formation is negligible, this shut-in pressure will remain constant and,

$$\sigma_{Hmin} \geq P_{isip}$$
$$\sigma_v = \gamma \cdot H \qquad (1)$$

where:

γ - rock weight gradient

H - depth to the fracturing horizon.

(ii) Vertical Stress as the Minimum Principal Stress

This situation generally occurs at shallow depths. A vertical fracture will initiate regardless of the value of σ_v due to the use of rubber packers which influence the induced stress distribution at the borehole wall. However, the fracture will "rotate" to become horizontal as it propagates away from the borehole and from its local influence.

Consequently, two shut-in pressures may be detected if the hydraulic fracturing tests are conducted with great care. The first shut-in pressure is associated with a vertical fracture while the second one corresponds to an horizontal fracture.

$$P_{s1} \geq P_{s2}$$

$$P_{s1} = \sigma_{Hmin} \qquad (2)$$

$$P_{s2} = \sigma_{v}$$

In this case, where fluid penetration into the formation is negligible,

$$P_b = 3\sigma_{Hmin} - \sigma_{Hmax} + T_o - P_o \quad (*) \qquad (3)$$

where (compression is taken positive):

P_b -- breakdown pressure

$\sigma_{Hmin} = P_{isip_1}$ -- minimum horizontal principal stress component

σ_{Hmax} -- maximum horizontal principal stress component

T_o -- apparent tensile strength

P_{isip} -- instantaneous shut-in pressure

P_o -- formation pore pressure

* The stresses calculated using this formula are total stresses

---

(*) This formula assumes no fluid penetration. Refinements to this approach are discussed subsequently.

3.2 FRACTURE MECHANICS APPROACH

In recent years, consideration of the hydraulic fracturing process in terms of classical elasticity, particularly the propagation phase, has been extended to include the presence of the fracture itself. Conventional analysis is probably incorrect for the determination of σ_{HMAX} because it ignores the mechanics of fracture initiation and fracture extension.

For example, growth of a crack inclined to the directions of the farfield in-situ stresses and subjected to pressure on its faces can be analysed by using fracture mechanics concepts where linear elasticity is assumed and consideration is devoted to the elevation of stresses near the crack tip.

A prerequisite is the assumption that plastic deformation and other non-linear effects near the crack tip are confined to a small region within a linear elastic field. In such a circumstance, the state of stress near the fracture tip can be characterized by the stress intensity factor K, or alternatively by the strain energy release rate, G. Cracks are expected to advance if the values of these parameters reach critical values characteristic of the material considered.

An Introduction to Fracture Mechanics

The presence of a crack (or a notch) in a body causes a redistribution of stress which may be estimated by methods of linear elastic stress analysis.

The surfaces of the crack are the dominating influence on the distribution of stresses near and around the tip. Other remote boundaries and loading forces affect only the intensity of the local stress field at the tip. Equations in terms of stress intensity factors have been formulated for stresses and displacements at crack tips. These stresses depend on stress intensity factors K_I, K_{II} and K_{III} which reflect the elevation of stress due to crack opening, sliding and tearing respectively.

One philosophy is that failure occurs when stress intensity factors reach critical values (i.e. K_{IC}) appropriate for a particular material. Other failure criteria are based on attainment of a maximum circumferential tensile stress, $\sigma_{\theta MAX}$, near the crack tip, attainment of a critical strain energy release rate or attainment of a critical strain energy density.

Various authors have considered the application of fracture mechanics to hydraulic fracturing analysis. Several approaches are outlined in Appendix C which is an excerpt from Numerical Modelling of Pressurized Fractures by J.-C. Roegiers and J.D. McLennan, October 1978.

Discussion of this topic by Abou Sayed et al, 1977*[1] is possibly the most relevant. Summarizing these authors' analysis ... Consider a

---

*1 Abou-Sayed, A.S., Brechtel, C.E., Clifton, R.J., In-Situ Stress Determination by Hydrofracturing - A Fracture Mechanics Approach; Terra Tek Report, TR77-60, July 1977.

pressurized crack which is oriented at an arbitrary angle α with respect to the direction of the horizontal stress σ_H of the far field system*1 (Figure 1). Extension of this existing crack at an arbitrary angle γ from the original inclination is associated wtih an energy-release rate $G(\gamma)$.

$$G(\gamma) = \frac{4(1-\nu^2)}{E} \left\{ \frac{1}{3+\cos^2\gamma} \right\} \left(\frac{\pi-\gamma}{\pi+\gamma}\right)^{\gamma/\pi} \left[(1+3\cos^2\gamma)\, K_I^2 + 8 \sin\gamma \cos\gamma\, K_I\, K_{II} + (9-5\cos^2\gamma)\, K_{II}^2 \right] \quad (4)$$

where $G(\gamma)$ - Strain energy release rate at an angle γ

ν - Poisson's ratio

E - Young's Modulus

K_I - Opening mode stress intensity factor

K_{II} - Sliding (shearing) mode stress intensity factor

Abou - Sayed et al.1977 provided the relationship between orientation of crack advance in a direction γ_{max} (in a direction where $G(\gamma)$ is a maximum) and the ratio of stress intensity factors K_{II}/K_I. The theory basically predicts that for $(\sigma_H - \sigma_V) \neq 0$ the crack tends to extend in a direction which is more nearly perpendicular to the direction of minimum compressive stress rather than along an existing crack.

This theory is based on isotropic assumptions. If anisotropy prevails, numerical analysis is required (e.g. finite element analysis).

---

*1 At the present time, mathematical complications encourage consideration of two dimensional situations.

If failure anisotropy is included, Abou-Sayed et al proposed the following failure criterion:

> *If $G(\alpha) - G_{HC}$ and $G(\gamma_{max}) < G_{VC}$, the inclined fracture will take a sharp turn and propagate along the bedding planes. On the other hand, if $G(\gamma_{max}) = G_{VC}$ and $G(\alpha) < G_{HC}$, then the crack extension will be in a direction inclined at angle γ_{max} to its original direction.*

where $G(\alpha)$ - strain energy release rate in original direction.

$G(\gamma_{max})$ - strain energy release rate in direction of additional extension

G_{HC} - critical strain energy release rate for horizontal extension

G_{VC} - critical strain energy release rate for vertical extension

Abou-Sayed et al, 1977, also offered a comparison between classical analysis and a fracture mechanics formulation:

$$\sigma_{Hmax} = 3P_s - P_b + \left(\frac{w^2 + 1}{w^2 - 1}\right) P_i - P_o \quad \text{(CLASSICAL)} \tag{5}$$

$$\sigma_{Hmax} = \frac{G}{(G-F)} P_s - \frac{F}{(G-F)} P_b + \frac{K_{IC}}{0.6\,(G-F)\sqrt{\pi L}} \quad \text{(FRACTURE MECHANICS)} \tag{6}$$

where: w - ratio of outer radius to inner radius in a laboratory burst test

P_i - burst pressure in laboratory test

G, F - tabulated parameters depending on the ratio of fracture length to borehole radius

L - fracture length

Cleary, 1979, has suggested an alternate formulation:

$$P_o^F + P_T \approx 3\sigma_M - \sigma_H - \zeta_{PT} + K_C/(0.56\sqrt{\pi \ell}) \qquad (7)$$

where:

P_o^F - the breakdown pressure for fast fracture (or jacketed borehole walls)

P_T - the ambient pore-fluid pressure

σ_M - the minimum in-situ horizontal stress (total)

σ_H - the maximum in-situ horizontal stress (total)

ζ - an effective stress parameter where $\sigma' = \sigma + \zeta p$, the prime denoting effective stress and p being a pore pressure. Tension is taken as positive.

K_C - critical opening mode stress intensity factor

ℓ - length of a pre-existing radial fracture.

IV. FIELD PROCEDURES

4.1 Fractured Horizons

It was desired to fracture a complete depth range in order to evaluate variation of stress with depth. It was also necessary to evaluate variation of stress in the individual formations. Caliper logs, from a previous hole survey formed the basis for selecting fracturing horizons in the Winnipeg and Deadwood sandstones. There was little flexibility in selecting a fracturing horizon in the Precambrian granite, due to the limited extent of the borehole into this formation.

Regardless, based on the logs, there seemed to be no predominant discontinuities in the pressurized horizons.

On the basis of the above considerations, the following horizons were tested (not all were successfully hydrofractured).

FRACTURE NUMBER	DEPTH (m)	FORMATION
1*	2211-2215	Precambrian
2*	2165-2170	Deadwood Sandstone (Cambrian)
3*	2062-2067	Winnipeg Sandstone (Middle Ordovician)
4	2069-2074	Winnipeg Sandstone (Middle Ordovician)
5*	2097-2102	Deadwood Sandstone (Middle Ordovician)

* Hydrofractured successfully

4.2 Field Instrumentation and Equipment

4.2.1 Straddle Packer

A straddle packer consists of two rubber seal elements mounted a set distance apart on a steel mandrel. These elements "straddle" a zone to be fractured. The zone is isolated from the rest of the hole by inflating these sealing elements, forcing them against the borehole wall. This sealed-off zone can then be pressurized until hydraulically induced fractures occur and/or pre-existing discontinuities open up.

The elements used were commercially available units from Lynes Inc. The diameter of the tool was 0.144 metres. A single packer of this variety is rated for 24.1 MPa (3500 psi) differential pressure in an open hole of 0.222 metres. The sealing elements were separated by 5.4 metres. The straddle packer assembly and auxilliary equipment for pressure measurement and coupling to the drill string is schematically shown in Figure 2.

The elements were lowered in order to "straddle" the fracturing interval*[1], were inflated and then sealed by twisting the tubing string at the surface. After several revolutions, a left-hand threaded split nut released, which in turn released the inner mandrel. The tubing string was then raised 0.23 metres, moving the injection ports of the inner mandrel in line with the ports of the outer mandrel, located between the sealing elements. The system was then open to the formation. After the fracturing sequence was completed, the tubing was lowered

---

*[1] For the fracture in the Precambrian, the limited depth to hole bottom required an alternate sealing arrangement, described in 4.2.2 .

.23 metres, moving the injection ports of the inner mandrel in line with the sealing elements and allowing for their deflation. The split nut was again engaged by this movement and the packer was ready to be moved to the next horizon.

4.2.2 Single Set Production - Injection Packer

This packer was used to inflate the lowest interval in the Precambrian. Essentially the principle and mode of operation is the same as for the straddle packer arrangement with the exception that the bottom of the hole serves as the lower seal. The packer configuration is shown in Figure 3.

4.2.3 Downhole Pressure Transducer

The downhole pressures were measured with a Kuster recording transducer mounted in the fracturing interval between the packers (or beneath the upper packer). The pressure transducer consists of three main components: a Bourdon-type pressure sensing element, a clock and a miniature recorder.

Pressure changes cause the Bourdon tube to expand or contract. These movements cause the attached recorder stylus to move. A coated brass chart records these stylus motions as etches in the chart coating. The chart moves past the stylus at a constant rate which is controlled by the spring-driven clock. Pressures are then determined by measuring the displacement of the etched line from the baseline of the chart.

4.2.4 The Pumping System

In order to attempt to pump at two vastly different flow rates, a multi-stage pumping programme was planned. It had been intended that

the first stage would involve pressurization using a high pressure - low volume pump (referred to later as "University of Toronto pump"). This was an air driven hydraulic pump manufactured by Teledyne Sprague. This pump operates on air pressure (0.69 MPa) and can discharge fluid at up to 42.1 MPa (6100 psi) at rates up to .9 USGPM. This unit was not extensively used because of leakage into the formation in excess of the pumping capabilities. As a result pumping with this pump resulted in pressure stabilization at a value below the breakdown pressure. At this time the larger pumping unit (referred to as Halliburton pump) was engaged. This HT-400 pumping unit was capable of flow rates of approximately 1910 gal/min at a maximum pressure of 96.6 MPa (14000 psi).

4.2.5 Surface Recording Equipment

All pressurization procedures were monitored using a continuous feed chart recorder and an X-Y recorder. These recorders responded to pressure sensed by a pressure transducer hooked into the surface iron. In addition, all pressurization was monitored from output of Bourdon type pressure gauges. Furthermore, the Halliburton pumping unit recorded line pressure, annulus pressure and flow rates.

4.2.6 Impression Packer

The impression packer was manufactured by Lynes, Inc., and consisted of a thick-walled rubber tube, wrapped with a soft semi-curved rubber sleeve.

The impression packer unit (Figure 4) is lowered on tubing to the fractured horizon. The element is then inflated, forcing the

soft rubber into all irregularities existing at the horizon, on the borehole wall. The impression packer is then deflated and allowed to return to its original shape. The impression of the borehole is retained on the soft rubber wrap.

Due to the long interval of fracturing, two impression packers (diameter 0.144 m and each sealing over 1.37 m) were used in tandem.

4.2.7 Single Shot Survey Instrument

An Eastman Canada single shot survey instrument was used to orient the fracture traces recorded on the impression packer. This instrument photographically recorded the azimuth and inclination of the borehole by photographing a clinometer-compass unit, giving the azimuth and inclination of a line scribed on the housing of the impression tool.

The instrument consists of three basic units: a clinometer-compass, a controlled light source with batteries and a clock, and the main frame containing the photographic mechanism. This unit is dropped down the string on a wire line. The device nests in a shoe in a known orientation. When the clock stops, the photograph is taken and the instrument is pulled out on the wire line.

4.3 Test Procedure

The tool string was lowered to the deepest horizon in order to fracture the granite. For this first fracture a single P.I. packer was used to seal off the top of the interval and the bottom of the hole was used as the lower seal. As this horizon is so deep, the generation of a horizontal fracture due to stress concentrations at the bottom of the hole is unlikely.

At this stage, using the Halliburton pump, the sealing element was inflated to approximately 3.4 MPa (500 psi). This pressure was held for several minutes in order to check the integrity of the O-rings in the packer. The packer was inflated in stages to 12 MPa (1750 psi) at which point the movements were made and ports to the formation were opened.

It was then attempted to pressurize the interval with the University of Toronto air-operated pump. As the flow rate is very small, breakdown did not occur, probably due to leakage into the formation. When breakdown did not occur, the well was "shut-in" (i.e. pumping was discontinued but the pressure was not released). Halliburton then pumped at $660 \cdot 10^{-6}$ m^3/sec (1/4 bbl/min) in order to breakdown the formation.

When breakdown appeared to occur, the well was "shut-in". The well remained shut-in for several minutes and then the cycle of pressurization was repeated. A series of breakdown-propagation-shut-in cycles was performed. After the last cycle the system was left shut-in for a longer period of time in order to study the pressure-decay behaviour.

For horizons tested above the Precambrian, the actual interval depths were determined from the core and caliper logs. For these intervals, the straddle packer arrangement was used.

During all phases, pressure and flow were monitored.

After fracturing, the packers were deflated. For the fracture in the Precambrian the packer was removed from the hole immediately after fracturing. For the straddle packers, it is ideally the case that after deflation, the tool string is raised to the next horizon and the same pressurization procedures are performed. Unfortunately packer failure at several intervals made it necessary to pull the entire tool string and use new packers more frequently than was desired.

The impressions of the fractures were taken by running the dual impression packers down the hole and inflating these in stages to a downhole pressure of 12 MPa at which point a shear pin burst. A check valve locked, maintaining this pressure in the packers. Therefore, it was no longer necessary to pump from the surface. At this point the orientation tool was dropped on a wireline, the photograph taken and the orientation tool pulled out on the wireline. After the film was developed the impression packer was deflated and removed from the hole.

Where possible, the orientation of the fracture trace was determined by measuring the relative angle between the fracture trace and the scribe line on the housing and from the film record determining the orientation of the scribe line.

V. LABORATORY TESTING AND RESULTS

5.1 Apparent Tensile Strength

5.1.1 Procedure

In order to estimate values of the tensile strength necessary for the calculation of σ_{HMAX}, laboratory hydraulic burst tests were peformed on cores obtained from the borehole. The cores, where possible, were machined to a length/diameter ratio of 2. The extremely friable nature of some of the samples made it sometimes necessary to use smaller L/D ratios.

A 6.4 mm diameter borehole was drilled through each sample (concentrically). In order to be able to use standard equipment to apply confining pressure to the samples, it was necessary to core smaller diameter samples (0.054 m diameter) from the available core prior to drilling the concentric interal borehole.

After preparation, samples were loaded axially, confined radially and the boreholes were pressurized internally until breakdown. The fluid used to pressurize the interval was very viscous hydraulic oil, selected in order to prevent penetration of borehole fluid into the sample (i.e. P_o did not increase due to the fracturing fluid). Based on the burst pressures measured in these simulated hydraulic fracturing tests, the tensile strength was estimated.

5.1.2 Computations

Thirty-five burst tests were performed. Of these, a percentage was done with no confining pressure (i.e. axial and borehole pressure

only). The others were done using a confining pressure. Despite the statistical scatter, the samples - when divided into similar rock types - display acceptably consistent behaviour.

Tensile strength values were determined from plots of $2\sigma_H$ versus P_b (σ_H being the confining pressure and P_b being the laboratory burst pressure). Specifically:

"In order to estimate the value of the major horizontal principal stress (σ_{Hmax}) the poroelastic relationship between the critical (breakdown) pressure (P_b) necessary to induce a vertical hydrofracture and the two horizontal principal stresses is used:

$$P_b - P_o = \frac{T + 3\sigma_{Hmin} - \sigma_{Hmax} - 2P_o}{K}$$

where compressive stresses are taken as positive and:

- *P_o is the pore pressure in the rock at the tested depth,*
- *T is the hydrofracturing tensile strength and is equal to P_b when $\sigma_{Hmin} = \sigma_{Hmax} = P_o = 0$ and $K = 1$,*
- *K is a poroelastic parameter which can be independently determined in the laboratory. The range of K is $1<K<2$. $K = 1$ when the formation is impermeable to the fracturing fluid. $K = 2$ when the rock matrix compressibility and the rock bulk compressibility are equal, or when the Poisson's ratio equals 0.5.*

In practice, the values of T and K can be derived from a plot of (P_c-P_o) versus $(3\sigma_{Hmin} - \sigma_{Hmax} - 2P_o)$ based on laboratory simulated hydrofracturing tests in which the principal stresses are known since they are the applied loads."[1]

In practice the analytical interpretation of K is somewhat more difficult than is outlined above. For example, K can be associated with the expression $\left[2 - \alpha \frac{1-2\nu}{1-\nu}\right]$

---

[1] Haimson, B.C.; The Hydrofracturing Stress Measuring Technique -- Method and Recent Field Results in the U.S.; ISRM Symposium, Sydney, Australia, August 1976.

where:

ν - Poisson's ratio

$$\alpha = 1 - \frac{C_r}{C_b}$$

C_r - compressibility of solids

C_b - compressibility of the bulk mass

The problem arises if K is considered both in terms of compressibility and permeability. For example, considering an impermeable granite: The permeability is very small implying $K \rightarrow 1$. However, the compressibility of the rock matrix material is approximately equal to the bulk compressibility implying $K = 2$.

In the present theory of hydraulic fracturing this discrepancy has not yet been entirely rationalized.

From the calculated values for T and K, the appropriate material properties are known for analysis.

Samples tested were visually divided into lithologically and structurally similar types. The test results are shown in Table 3.

With appropriate analysis, the data has been reduced to give values for the apparent tensile strength T_o and the poroelastic parameter K. These are indicated in Table 4.

TABLE 3

RAW DATA FOR LABORATORY HYDRAULIC FRACTURING BURST TESTS

SAMPLE *1	DEPTH (m)	DESCRIPTION	σ_{CONF} (MPa)	σ_{AXIAL} (MPa)	P_b (MPa)
247	2210.6-2211.0	Granite	3.10	19.12	25.86
247	2210.6-2211.0	"	0	12.61	22.07
246	2209.6-2210.4	"	0	19.12	23.48
244	2209.0-2209.5	"	2.69	19.22	23.34
244	2209.0-2209.5	"	4.97	19.22	29.62
215	2103.8-2104.0	Fine Grained, Well-Cemented Quartz Sandstone	3.59	19.22	20.76
214	2103.4-2103.6	"	6.21	19.28	30.21
214	2103.4-2103.6	"	0	12.71	14.00
196	2099.0-2099.2	Moderately Clean, Fine to Medium Quartz Sandstone (may be thin argillaceous or pyritic bands)	0	6.30	6.66
195	2098.8-2099.0	"	9.83	19.22	11.38
194	2098.5-2098.7	"	10.34	22.69	27.76
190	2097.6-2097.8	"	11.90	26.79	23.28
188	2097.1-2097.3	"	11.03	21.11	20.10
185	2096.3-2096.5	"	3.17	18.90	17.17
185	2096.3-2096.5	"	4.14	17.86	13.03
176	2081.0-2081.2	"	7.24	19.12	20.69
174	2080.4-2080.6	"	6.34	18.70	23.93
164	2077.8-2078.0	"	0	5.67	7.52
154	2075.4-2075.6	"	7.24	25.00	27.24
134	2069.9-2070.1	Medium Grained Sandstone	8.45	18.90	20.34
129	2068.7 2068.9	"	22.76	37.81	25.52
127	2068.2-2068.4	"	0	4.20	1.03
108	2059.4-2059.6	Grey-white, medium grained, friable sandstone	0	3.99	4.76
106	2058.8-2059.0	"	17.59	25.31	20.34
105	2058.6-2058.8	"	11.03	18.70	13.10
101	2057.5-2057.7	"	13.45	23.63	20.69
98	2056.8-2057.0	"	3.45	13.03	11.38
97	2056.6-2056.8	"	6.21	18.90	15.86
88	2054.0-2054.2	"	0	2.10	2.55
76	2050.6-2050.8	Dirty brown, medium grained, quartz sandstone	13.79	21.01	26.17
71	2049.2-2049.4	"	7.24	12.61	11.79
67	2048.0-2048.2	"	6.90	12.81	12.76
58	2045.5 2045.7	"	7.93	19.96	24.83

*1 Sample designation is according to the University of Regina labelling system except that the "R" is deleted from the designation (i.e. 123 rather than R-123).

TABLE 4

LABORATORY TENSILE STRENGTHS
AND POROELASTIC CONSTANTS

GROUP	SAMPLES	DEPTH RANGE (m)	T_o (MPa)	K
A (Granite)	247,246,244	2209.0-2211.0	25.74	1.2
B (Fine Grained, Well Cemented, Quartz Sandstone)	215,214	2103.4-2104.0	19.05	1.0
C (Moderately Clean, Fine to Medium, Quartz Sandstone)	196,195,194 190,188,185 176,174,164,154	2075.4-2098.7	17.82	1.7
D (Medium Grained Sandstone)	134,129,127	2068.2-2070.1	4.05	1.6
E (Gray-White, Medium Grained, Friable Sandstone)	108, 106,105, 101,98,97,88	2054.0-2059.6	12.72	2.0
F (Dirty Brown, Medium Grained, Quartz Sandstone)	76,71,67,58	2045.5-2050.8	10.34	1.5

From this information it is now necessary to assess the appropriate parameters for the individual fracturing intervals. Table 5 indicates the selected parameters.

TABLE 5

SELECTED VALUES FOR THE TENSILE STRENGTH AND POROELASTIC CONSTANT

FRACTURE NUMBER	DEPTH (m)	T_o (MPa)	K	COMMENTS
1	2211-2215	25.74	1.2	-
2	2165-2170	19.05	1.0	Assumed as B in Table 4
3	2062-2067	8.39	1.8	Average of D and E in Table 4
4	2069-2074	10.94	1.65	Average of C and D in Table 4
5	2097-2102	18.44	1.35	Average of B and C in Table 4

In terms of the other poroelastic parameter, α, after Haimson 1968 ..., it may also be backcalculated from K measured in the burst tests. In addition, based on a limited number of laboratory uniaxial compression tests, porosity measurements and judicious selection of representative properties based on characteristics of similar rock materials, K and α have been calculated from first principles. The following table indicates the results.

TABLE 6

MATERIAL PROPERTIES

SAMPLE	G (MPa)	ν	ν_o	k (md)	K_s(MPa)	K_f(MPa)	K(MPa)	B	ν_u	η	c(cm^2)	$\alpha=1-\frac{K}{K_s}$	K*1
244,246,247	16850	.26	.015	$2x10^{-4}$	45400	3300	29480	.74	.31	.11	.15	.35	1.77
214,215	12200	.15	.06	1	36000	3300	13350	.74	.29	.26	220	.63	1.70
154,164,174, 176,185,188, 190,194,195, 196	11400	.15	.07	5	36000	3300	12478	.73	.36	.37	790	.65	1.46
127,129,134	2600	.20	.15	200	36000	3300	3464	.86	.27	.12	$220x10^4$	.90	1.33
88,97,101 105,106,108	8100	.20	.09	50	36000	3300	10790	.72	.33	.25	$1x10^4$	.70	1.48
58,67,71,76	7400	.18	.10	100	36000	3300	8528	.76	.38	.35	$1.2x10^4$	.76	1.31

where: G - Shear Modulus

ν - Poisson's Ratio

ν_o - Porosity

k - Permeability

K_s - Bulk modulus of solids

K_f - Bulk modulus of fluids

K - Bulk modulus of the rock

B - Pore Pressure coefficient $B = \dfrac{1/K - 1/K_s}{\nu_o/K_f + 1/K - 1/K_s - \nu_o/K_s}$

ν_u - Undrained Poisson's Ratio $\nu_u = \dfrac{3\nu + B(1-2\nu)(1-K/K_s)}{3 - B(1-2\nu)(1-K/K_s)}$

η - Plane strain parameter $\eta = 3(\nu_u-\nu)/[2B(1+\nu_u)(1-\nu)]$

c - Diffusivity $c = \dfrac{k}{\mu}\left[\dfrac{2G(1-\nu)}{(1-2\nu)}\right]\left[\dfrac{B^2(1+\nu_u)^2(1-2\nu)}{9(1-\nu_u)(\nu_u-\nu)}\right]$

(After Rice and Cleary, 1976)

*1 This "K" indicates Haimson's poroelastic parameter

The poroelastic parameters detemined from the burst tests and from basic material properties are summarized below, for each fracture interval.

TABLE 7

POROELASTIC PARAMETERS

INTERVAL	DEPTH (m)	T_o (MPa)	BURST TEST		MATERIAL PROPERTIES	
			α	K	α	K
1	2211-2215	25.74	1.23*[1]	1.2	.35	1.77
2	2165-2170	19.05	1.21*[1]	1.0	.63	1.48
3	2062-2067	8.39	.27	1.8	.80	1.40
4	2069-2074	10.94	.44	1.65	.78	1.39
5	2097-2102	18.44	.79	.79	.64	1.47

*[1] α has been calculated from K. By definition α cannot exceed 1. These values arise because of the value of Poisson's ratio used in the calculations.

The approach to overcome discrepancies in poroelastic parameters is uncertain. The most logical approach is to evaluate all possibilities in the stress calculations and through judicious interpretation select a representative range of stress values.

5.2 Critical Stress Intensity Factor

5.2.1 Procedure

Two separate testing procedures were used to estimate the critical stress intensity factors. These were:

(i) Hydraulic burst tests on prenoteched specimens.

(ii) Short rod technique.

The specimens for the hydraulic burst tests were thick-walled cylinders with an outer radius of 27 mm and an inner radius of 3.18 mm. Two radially opposed prenotches (with a depth of approximately 1.6 mm) were cut along the entire length of the borehole.

The specimens were loaded axially and confining pressure was applied by pressurization behind a urethane membrane. The applied loading was designed to simulate anticipated *in situ* stress conditions. The internal borehole was pressurized until breakdown occurred. The pressurization fluid was viscous oil selected in order to prevent penetration of fluid into the specimens during testing. Fracture toughness (K_{IC}) was calculated from available formulae (Tada et al, 1973).

Four specimens were prepared. The friable nature of many of the samples prevented satisfactory slots being cut in three of the specimens. Consequently, only one sample is regarded as indicating representative values.

The Short Rod Technique (Refer to Figure 5) allows the measurement of the plane strain critical stress intensity factor K_{IC}. Advantages of this technique are that:

(i) the specimen has a geometry favouring plane strain conditions.

(ii) the need for pre-cracking is reduced.

(iii) sample size is small enough that measurements of anisotropic behaviour are possible.

Samples are prepared by cutting a narrow chevron notch in a plane parallel to the axis of the core. The core is pulled apart at a slow, controlled displacement rate so that splitting of the chevron notch is encouraged. The load applied to the sample is electronically recorded. Simultaneously displacement across the sawn crack is recorded (accuracy of .001 mm). This is accomplished with a "clip-gauge" measuring displacement between two plattens epoxied to the rock face on either side of the sawn cut.

The load is increased slowly until a crack initiates at the tip of the "V". Initially crack growth is stable and each incremental load corresponds to further fracture propagation. When the crack attains a critical length, this trend is reversed and the load decreases with increasing crack length.

5.2.2 Computations

One analytical interpretation of the results, proposed by Barker*[1] 1977, is:

$$K_{IC} = \frac{AF_c}{B^{3/2}} \qquad (8)$$

---

*[1] Barker, L.M.; A Simplified Method for Measuring Plane Strain Fracture Toughness; Engineering Fracture Mechanics, 1977, Vol. 9, pp. 361-369.

where:

K_{IC} - critical stress intensity factor

A - a material independent parameter, found to be approxiamtely 20.8

B - specimen diameter

F_c - maximum load

Unfortunately, the parameter A may be geometrically sensitive. To overcome this, an alternate approach is to analyse the samples as "compact specimens". Computations are based on formulae proposed by Srawley and Gross, 1972*[1], where appropriate parameters for particular geometry and loading conditions are outlined.

Finally results were also analysed using compilance calculations*[2]. Once the increase of compilance with crack length has been computed, the stress intensity factors can be calculated from:

$$G = \frac{P^2}{2B} \frac{\partial C}{\partial a} \tag{9}$$

$$K_I = \frac{GE}{1-\nu^2} \tag{10}$$

---

*1 Srawley, J.E., Gross, B.; Stress Intensity Factors for Bend and Compact Specimens; Compenduim, Eng. Frac. Mech., 1972, Vol. 4, pp. 587-589.

*2 The compilance is the ratio at the point of maximum load of the displacement to the load.

where:

G - strain energy release rate

B - specimen diameter

K_I - opening mode stress intensity

E - Young's modulus

ν - Poisson's ratio

The compilance method and Barker's calculations appeared to give inferior results compared to the "compact specimen" approach. Representative values are summarized below:

TABLE 8

STRESS INTENSITY FACTORS

GROUP	SAMPLE	K_I (MPa-m$^{-3/2}$) (Srawley and Gross, 1972)	K_I (MPa-m$^{-3/2}$) (Barker, 1976)
A*1	241	.39	.24
	241	1.4	.47
	242	.79	.46
	243	.32-.36	.46
B	243	1.9-2.1	2.4
	244	4.4	1.2
C	201	.42-.43	.30
	195	.30	.21
	194	.28-.31	.41
	190	1.6	.68
	188	.86-.87	.58
D	164	.67-.75	.95
	154	.48-.49	.35
	153	.55	.26
E	134	.15	.059
	133	.080	.053
	129	.016-.018	.022
F	98	.099	.042
	97	.069-.070	.046
	94	.050-.056	.076
G	71	.067	.037
	67	.089-.099	.13
	62	.56-.57	.42
	58	.41	.18

*1 This is weathered granitic material from near the Precambrian contact. It was not amendable for producing long enough samples for burst tests. While it lay outside the pressurized interval, it may have affected latter stages of propagation.

The groups in the above table were selected to incorporate samples of similar lithology and structure. From these results appropriate stress intensity factors for the individual fracture intervals were selected (Table 9).

TABLE 9

REPRESENTATIVE STRESS INTENSITY FACTORS

FRACTURE NUMBER	DEPTH (m)	OPENING MODE CRITICAL STRESS INTENSITY FACTOR, K_{IC} ($MPa - m^{-3/2}$)		
		ABSOLUTE RANGE	MINIMUM	AVERAGE
1	2211-2215	1.9-4.4	1.9	3.2
2	2165-2170	.28-1.6	.28	.70
3	2062-2067	.016-.15	.016	.078
4	2069-2074	.016-.75	.016	.33
5	2097-2102	.28-1.6	.28	.70

In all calcualtions the average value of K_{IC} has been used because it is

(i) Most representative of the entire interval.

(ii) Probably conservatively small enough due to inevitable sample damage during the sampling procedure and during transportation.

VI. DATA ANALYSIS

6.1 Introduction

The first fracturing interval was in the Precambrian (using the single packer). Next an interval in the Deadwood was fractured. Two fractures (one of which was successful) were then attempted in the in the Winnipeg formation. Finally another fracture was performed in the Deadwood formation. The fractures were not propped and due to conditions which arose in the field none of the fractures were filled with the very viscous gel.

6.2 In-Situ Stresses*[1]

Table 10 synthesizes the raw results of the downhole and the surface recordings. Pressure-time diagrams are presented in Appendix A. Appendix B contains reproductions of the downhole pressure-time plots.

Table 11 indicates the calculated *in situ* stresses, based on the assumption of tensile strengths typical of rocks of the nature encountered in this hole:

Tensile Strength T_o (MPa)	Rock
21	Granite
3.5	Sandstone

Table 12 tabulates *in situ* stresses based on tensile strengths derived from the laboratory testing programme.

Finally, Tables 13-15 outline *in situ* stresses based on measured (laboratory) values of fracture toughness using fracture mechanics considerations.

---

*[1] The stresses tabulated are total stresses.

TABLE 10

RECORDED HYDROFRACTURING PRESSURES

FRACTURE NUMBER	DEPTH*1 (m)	FORMATION PRESSURE P_o (MPa)		INITIAL BREAKDOWN PRESSURE P_{bi} (MPa)		INSTANTANEOUS SHUT-IN PRESSURE Pisip (MPa)	
		ESTIMATED*2 (to surface)	DOWNHOLE	SURFACE PLUS FORMATION PRESSURE	DOWNHOLE	SURFACE PLUS FORMATION PRESSURE	DOWNHOLE
1	2213	23.87	22.16	42.66	39.90	29.56-35.42	30.54
2	2168	23.38	21.13	33.72	32.43	30.62	28.01
3	2065	22.34	19.16	29.93	--	25.10	--
5	2100	22.65	--	51.62	--	33.68	--

*1 This is the depth to the centre of the fracturing interval.

*2 Based on a specific gravity of 1.1 for pore fluid.

TABLE 11 *1

IN SITU STRESSES (BASED ON ASSUMED VALUES OF TENSILE STRENGTH, T_o)

FRACTURE NUMBER	DEPTH (m)	POROELASTIC PARAMETERS FROM BURST TESTS			POROELASTIC PARAMETERS FROM MATERIAL PROPERTIES			ASSUMING K=1			ORIENTATION OF σ_{HMAX}
		σ_{HMAX} (MPa)	σ_{HMIN} (MPa)	σ_v = .025 x DEPTH (MPa)	σ_{HMAX} (MPa)	σ_{HMIN} (MPa)	σ_v = .025 x DEPTH (MPa)	σ_{HMAX} (MPa)	σ_{HMIN} (MPa)	σ_v = .025xDEPTH (MPa)	
1	2213	56.97	29.56-35.42	55.08	46.28	29.56-35.42	55.08	60.73	29.56-35.42	55.08	-
2	2168	38.26	30.62	53.96	33.28	30.62	53.96	38.26	30.62	53.96	N61W
3	2065	20.46	25.10	51.40	23.49	25.10	51.40	26.53	25.10	51.40	W20S
5	2100	20.13	33.68	52.27	16.59	33.68	52.27	30.27	33.68	52.27	-

*1 Inherent inaccuracies in any hydraulic fracturing procedure do not justify calculations of stresses to as many significant figures as shown.

TABLE 12

IN SITU STRESSES (TENSILE STRENGTH BASED ON LABORATORY MEASUREMENTS)

FRACTURE NUMBER	DEPTH (m)	POROELASTIC PARAMETERS FROM BURST TESTS			POROELASTIC PARAMETERS FROM MATERIAL PROPERTIES			ASSUMING K=1			ORIENTATION OF σ_{HMAX}
		σ_{HMAX} (MPa)	σ_{HMIN} (MPa)	σ_v = .025 x DEPTH (MPa)	σ_{HMAX} (MPa)	σ_{HMIN} (MPa)	σ_v = .025 x DEPTH (MPa)	σ_{HMAX} (MPa)	σ_{HMIN} (MPa)	σ_v = .025xDEPTH (MPa)	
1	2213	61.71	20.56-35.42	55.08	51.00	20.56-35.42	55.08	65.47	20.56-35.42	55.08	-
2	2168	53.81	30.62	53.96	48.83	30.62	53.96	53.81	30.62	53.96	N61W
3	2065	25.35	25.10	51.40	28.38	25.10	51.40	31.42	25.10	51.40	W20S
5	2100	35.07	33.68	52.27	31.53	33.68	52.27	45.21	33.68	52.27	-

TABLE 13 (Refer to Figure 9)

IN SITU STRESSES (FRACTURE MECHANICS APPROACH)

FRACTURE NUMBER	DEPTH (m)	σ_{HMAX} (MPa) *1			σ_{HMIN} (MPa)	σ_v (MPa)	ORIENTATION
		ℓ = .5mm	ℓ = 1.0mm	ℓ = 25mm			
1	2213	155.51	116.09	88.85	35.42	55.08	-
2	2168	53.85	45.23	39.27	30.62	53.96	N61W
3	2065	18.72	17.76	17.10	25.10	51.40	W20S
5	2100	27.23	18.61	12.65	33.68	52.27	-

*1 Abou-Sayed proposed that, for a pressurized borehole intersected by a pre-existing fracture of preferred orientation, a more representative formulation for σ_1 is:

$$\sigma_1 \approx 3\ \text{Pisip} - 2P_b + \frac{K_{IC}}{\sqrt{\pi \ell}\ (0.6)}$$

where: ℓ - crack length for one arm of a diametrically opposed crack
K_{IC} - critical stress intensity factor

Two predominant difficulties are that it is difficult to estimate the length of pre-fractures (a range of fracture lengths has been evaluated) AND the analysis presupposes no fluid penetration.

TABLE 14 (Refer to Figure 10)

IN SITU STRESSES (FRACTURE MECHANICS APPROACH)

FRACTURE NUMBER	DEPTH (m)	σ_{HMAX} (MPa) *1			σ_{HMIN} (MPa)	σ_v (MPa)	ORIENTATION
		ℓ = .5mm	ℓ = 1.0mm	ℓ = 25mm			
1	2213	183.91	141.68	112.49	35.42	55.08	-
2	2168	66.29	57.06	50.67	30.62	53.96	N61W
3	2065	26.54	25.52	24.81	25.10	51.40	W20S
5	2100	59.37	49.07	42.68	33.68	52.27	-

*1 Cleary proposed that, for a pressurized borehole intersected by a pre-existing fracture, a formulation (where total stress is equal to effective stress) is:

$$\sigma_1 \approx 3\ Pisip - P_b - P_o + \frac{K_{IC}}{\sqrt{\pi \ell}\ (.56)}$$

where: ℓ - crack length for one arm of a diametrically opposed crack
K_{IC} - critical stress intensity factor

This formulation is for rapid breakdown with a consequently limited amount of fluid penetration. Analysis of Fracture Number 3 in this manner may not be accurate.

The predominant difficulty is in estimating the length of pre-existing fractures. A range of fracture lengths has been evaluated.

TABLE 15 (Refer to Figure 11)

IN SITU STRESSES (FRACTURE MECHANICS APPROACH)

FRACTURE NUMBER	DEPTH (m)	σ_{HMAX} (MPa) *1			σ_{HMIN} (MPa)	σ_v (MPa)	ORIENTATION
		ℓ = .5mm	ℓ = 1.0mm	ℓ = 25mm			
1	2213	160.04	117.81	88.62	35.42	55.08	-
2	2168	42.91	33.68	27.29	30.62	53.96	N61W
3	2065	4.20	3.18	2.47	25.10	51.40	W20S
5	2100	36.72	26.42	20.03	33.68	52.27	-

*1 Cleary proposed that, for a pressurized borehole intersected by a pre-existing fracture, a formulation (where $\sigma' = \sigma - p$) is:

$$\sigma_1 \approx 3\ Pisip - P_b - 2P_o + \frac{K_{IC}}{\sqrt{\pi \ell}\ (.56)}$$

where: ℓ - crack length for one arm of a diametrically opposed crack
K_{IC} - critical stress intensity factor

This formulation is for rapid breakdown with a consequently limited amount of fluid penetration. Analysis of Fracture Number 3 in this manner may not be accurate.

The predominant difficulty is in estimating the length of pre-existing fractures. A range of fracture lengths has been evaluated.

6.3 Fracture Orientation

At these depths all fractures are generally vertical. It is unlikely that bedding plane anisotropy will have disrupted this trend.

The final column in each of the foregoing tables summarizes the fracture orientations as determined from the impression packers and the downhole orientation surveys.

The quality of the impressions was quite disappointing. The tendency was for most of the rubber wrap to be scraped off the impression packers as the tool was pulled into the casing on the return trip. Nevertheless, some interpretation was possible and is documented.

6.4 Discussion

6.4.1 Variation of Horizontal Stress With Depth

Figures 6 and 7 indicate the variation of σ_{HMAX} and σ_{HMIN} with depth.

The minimum horizontal principal stress appears to have a relatively constant gradient with depth. This is substantiated by the variation of the ratio of σ_{HMIN}/σ_V shown in the following table. σ_V has been calculated as the weight of overlying rock, a valid assumption based on the numerous deep stress measurements made previously at other localities.

TABLE 16

σ_{HMIN}/σ_v

FRACTURE NUMBER	DEPTH (m)	σ_{HMIN} (MPa)	σ_v (MPa)	σ_{HMIN}/σ_v
1	2213	35.42	55.08	.64
2	2168	30.62	53.96	.57
3	2065	25.10	51.40	.48
5	2100	33.68	52.27	.64
			AVERAGE	.58

This gradient seems quite reasonable. Even in terms of the very simplified theoretical relationship that $\sigma_H = \sigma_v \frac{\nu}{1-\nu}$, the back calculated value of ν is 0.37 which is not too unrealistic.

In terms of the maximum horizontal principal stress, the variation with depth is somewhat more complicated. This could be due to:

(a) Estimations of σ_{HMAX} which are inherently somewhat more inaccurate due to the presence of additional parameters in the calculations.

(b) Lithological variations.

(c) Past tectonic activity.

Figure 6 indicates that regardless of the assumptions made concerning the poroelastic parameters, the basic trend is the same. It should be pointed out however that the highest quality of available information is for the curve obtained, based on burst test results. As such, this has been adopted as representing the variation of σ_{HMAX}.

Over the relatively small depth span σ_{HMAX} also shows a very steep gradient. It is uncertain what the influence of the Cambrian-Precambrian contact has on this gradient. The variation of σ_{HMAX} with respect to

the vertical stress σ_v is indicated in Table 17.

TABLE 17

σ_{HMAX}/σ_v

FRACTURE NUMBER	DEPTH (m)	σ_{HMAX} *1 (MPa)	σ_v (MPa)	σ_{HMAX}/σ_v
1	2213	61.71	55.08	1.12
2	2168	53.81	53.96	.99
3	2065	23.35	51.40	.45
5	2100	35.07	52.27	.67

*1 Refer to Table 12 (based on a limited number of measurements)

It would appear from the above table and Figure 8 , which indicates the variation of all the principal stresses with depth, that the Deadwood sandstone may be a zone of transition from a state of stress in the Winnipeg where $\sigma_v > \sigma_{HMAX} \approx \sigma_{HMIN}$ to a situation in the upper part of the Precambrian where $\sigma_{HMAX} > \sigma_v > \sigma_{HMIN}$.

6.4.2 Orientation and Regional Stress "Picture"

Figures 12 through 16 indicate the stress measurements at this site in comparison with measurements elsewhere. Figure 17 indicates stress measurement values at other sites in western North America, and shows relatively good agreement.

From the orientations measured, the approximately E-W trend of σ_{HMAX} is not unreasonable, when viewed in conjunction with other previous measurements (Figure 18).

6.4.3 Fracture Mechanics Considerations

Tables 13 to 15 are simply alternative approaches to the calculation of σ_{HMAX}. These, however, incorporate the presence of minute flaws intersecting the borehole. All the tables are based on breakdown after a short period of time so that there is no penetration of fluid. A further dramatic disadvantage of using calculations of this nature is in ascertaining the length (and possibly the persistance along the borehole) of these critical pre-existing cracks.

Since no definite measurement of the length of influential pre-existing discontinuities is readily available, only a qualitative review of this data is possible. Nevertheless, Figures 9 to 11 indicate that the general trends for conventional and fracture mechanics approaches are roughly the same. The figures do however highlight the strong influence that the presence of fractures can have. This is particularly true in the "intact" granite. However, based on the present state-of-the-art and available information the conventional analysis will be considered as valid. It is interesting to note the relatively good agreement in Figure 11 between both analyses for a 0.5 mm deep crack (a feasible length considering the grain sizes). The discrepancy in the granitic zone could easily be less if it is realized that the fracture toughness used here is an upper limit. A value for K_{IC} in this horizon of 3.2 MPa - $m^{-3/2}$ (an average) was used rather than 1.9 MPa - $m^{-3/2}$ (the measured minimum). If the minimum value in this horizon is used, the predicted stress values in the granitic horizon would be (for the equivalent computations to those summarized in Figure 11):

CRACK LENGTH (m)	σ_{HMAX} (MPa)
5×10^{-4}	125.33
10^{-3}	100.26
25×10^{-3}	82.93

These values are closer to σ_{HMAX} = 61.71 MPa calculated using conventional techniques.

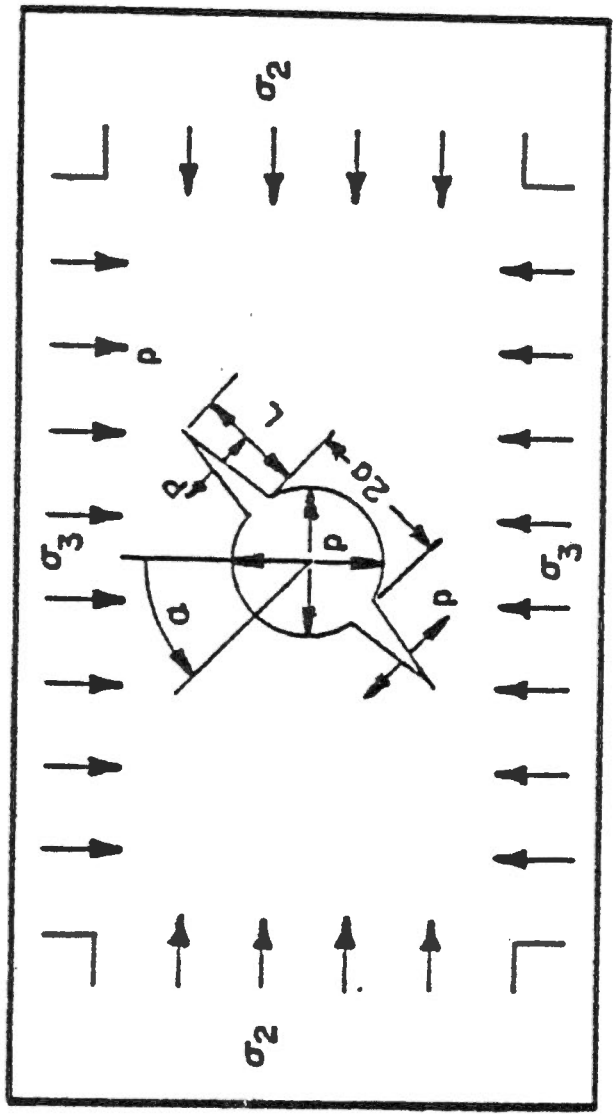

FIGURE 1 : (AFTER ABOU-SAYED ET AL, 1977)

INTERNALLY PRESSURIZED CRACKED BOREHOLE
UNDER FAR FIELD STRESS.

FIGURE 2: STRADDLE PACKER ASSEMBLY
(not to scale)

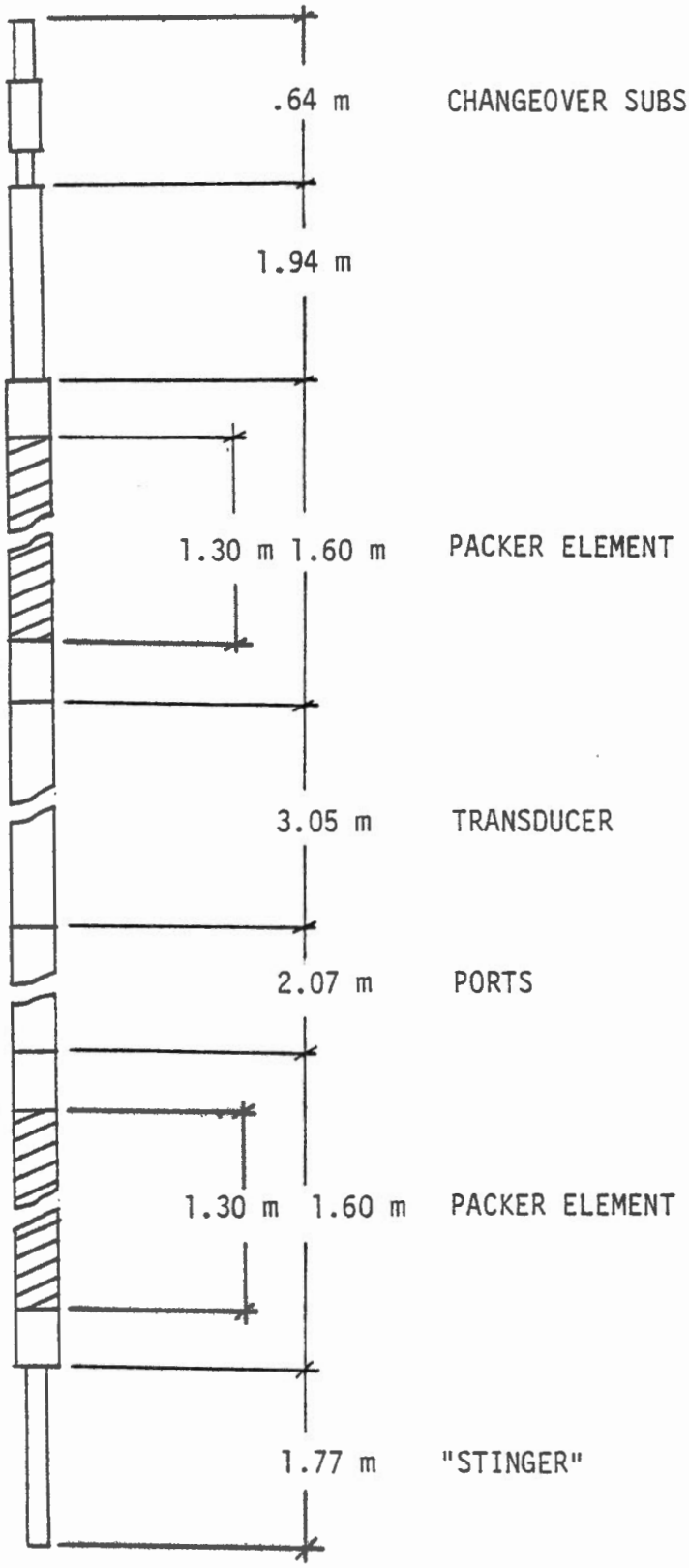

FIGURE 3: PRODUCTION INJECTION PACKER (not to scale)
(used in the Precambrian interval)

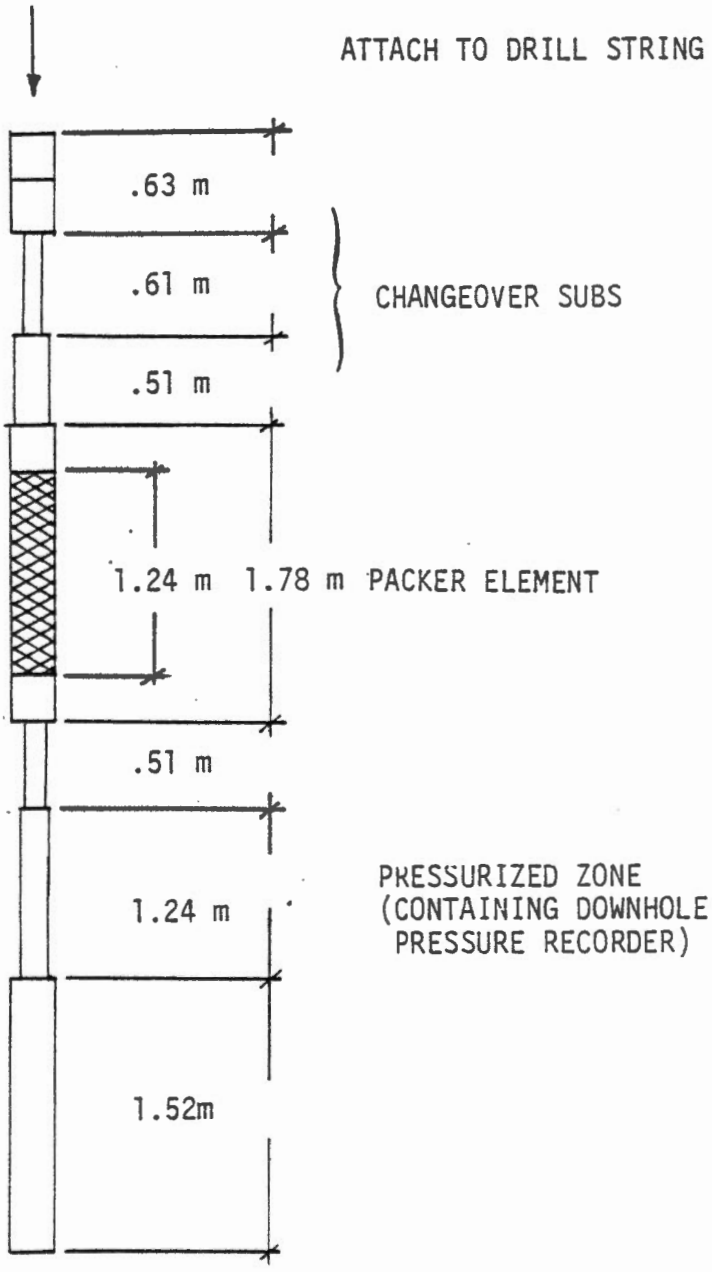

FIGURE 4: IMPRESSION PACKERS (not to scale)

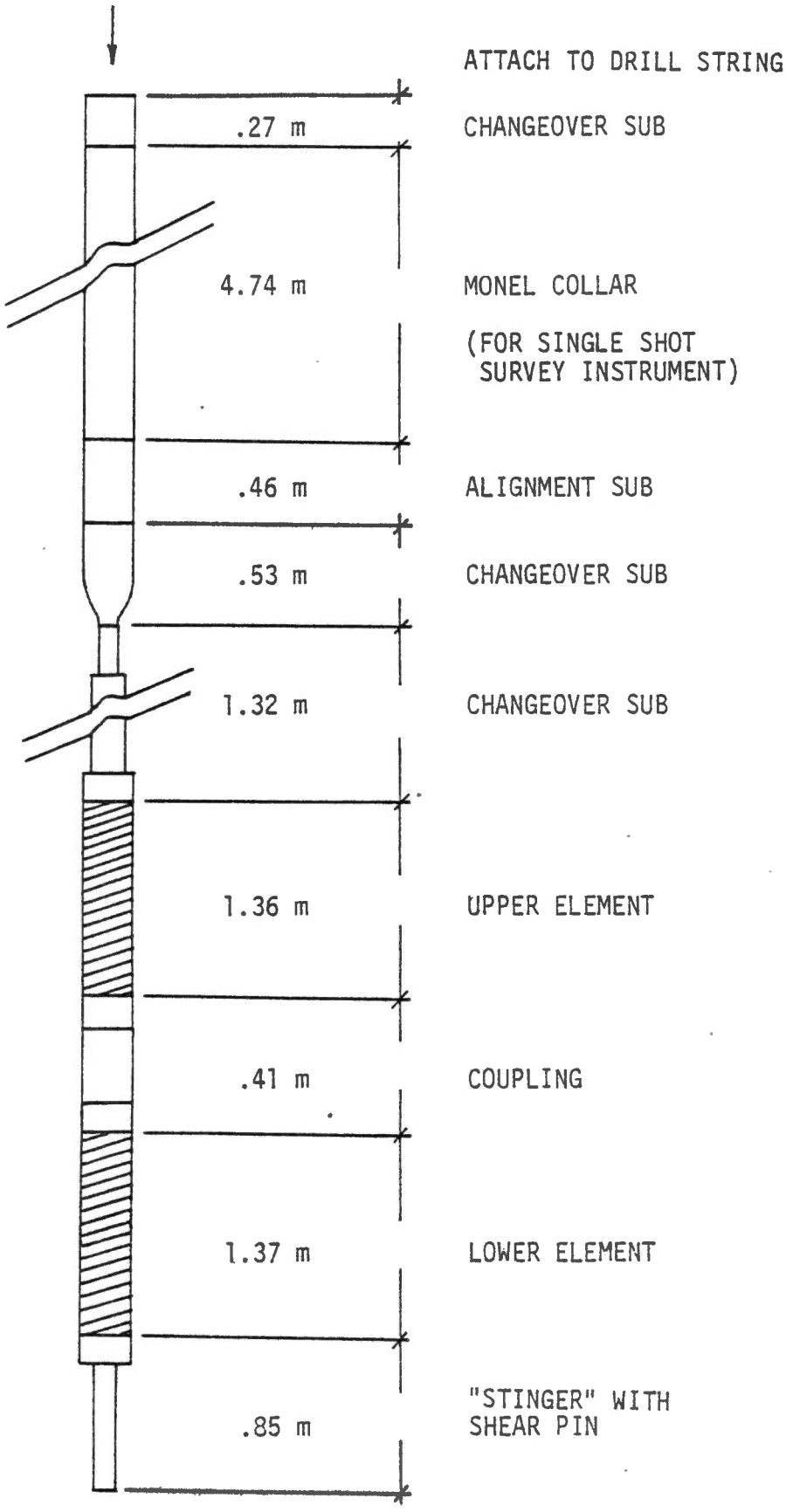

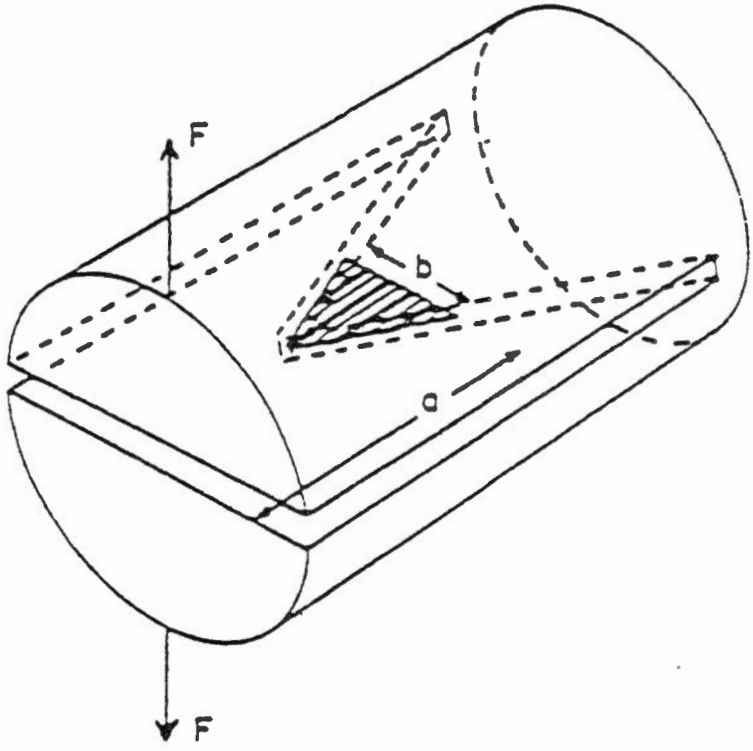

F - Load

b - Instantaeous Crack Width (Shaded area denotes crack)

FIGURE 5: Short Rod Specimen Configuration (After Barker, 1976)

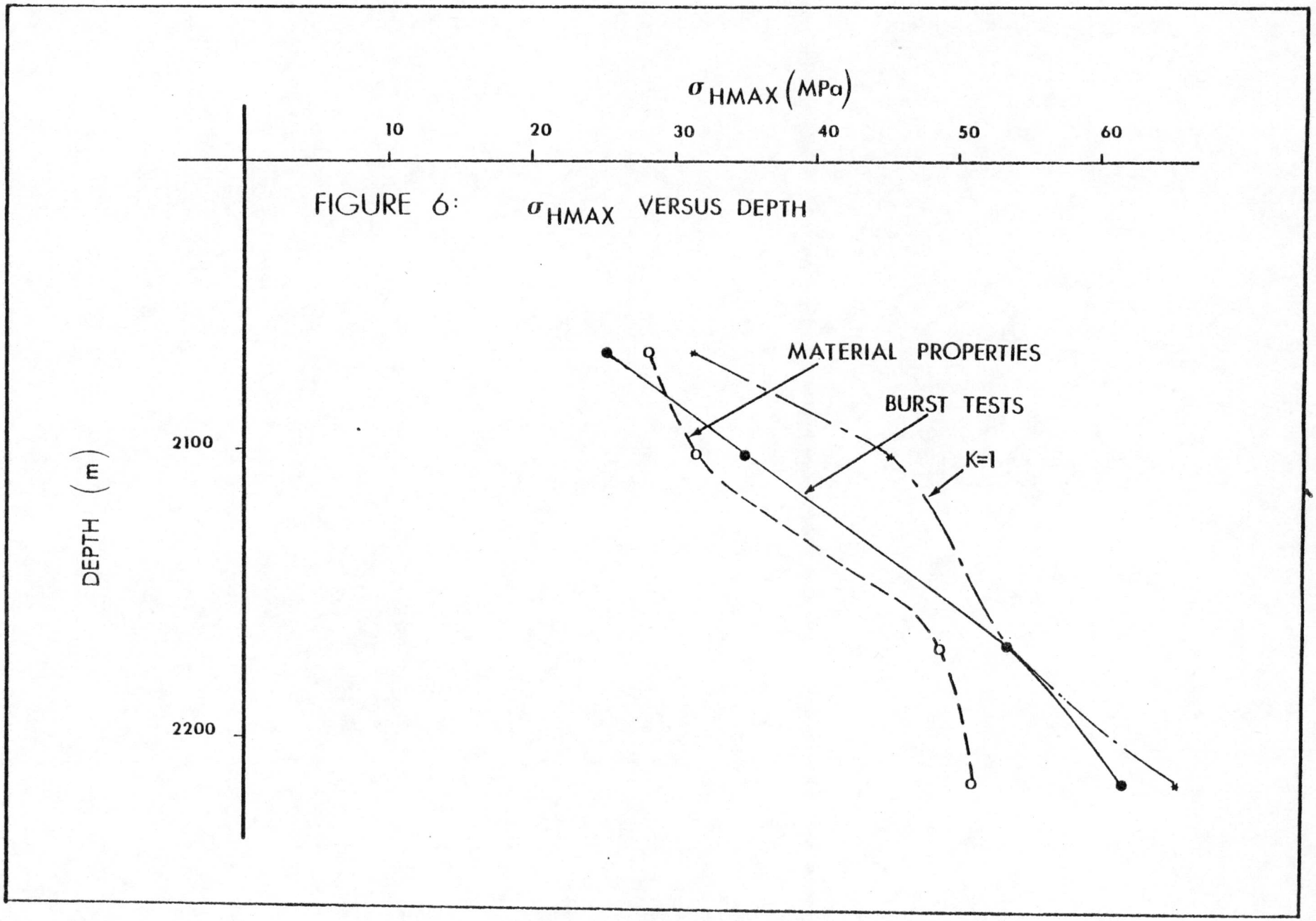

FIGURE 6: σ_{HMAX} VERSUS DEPTH

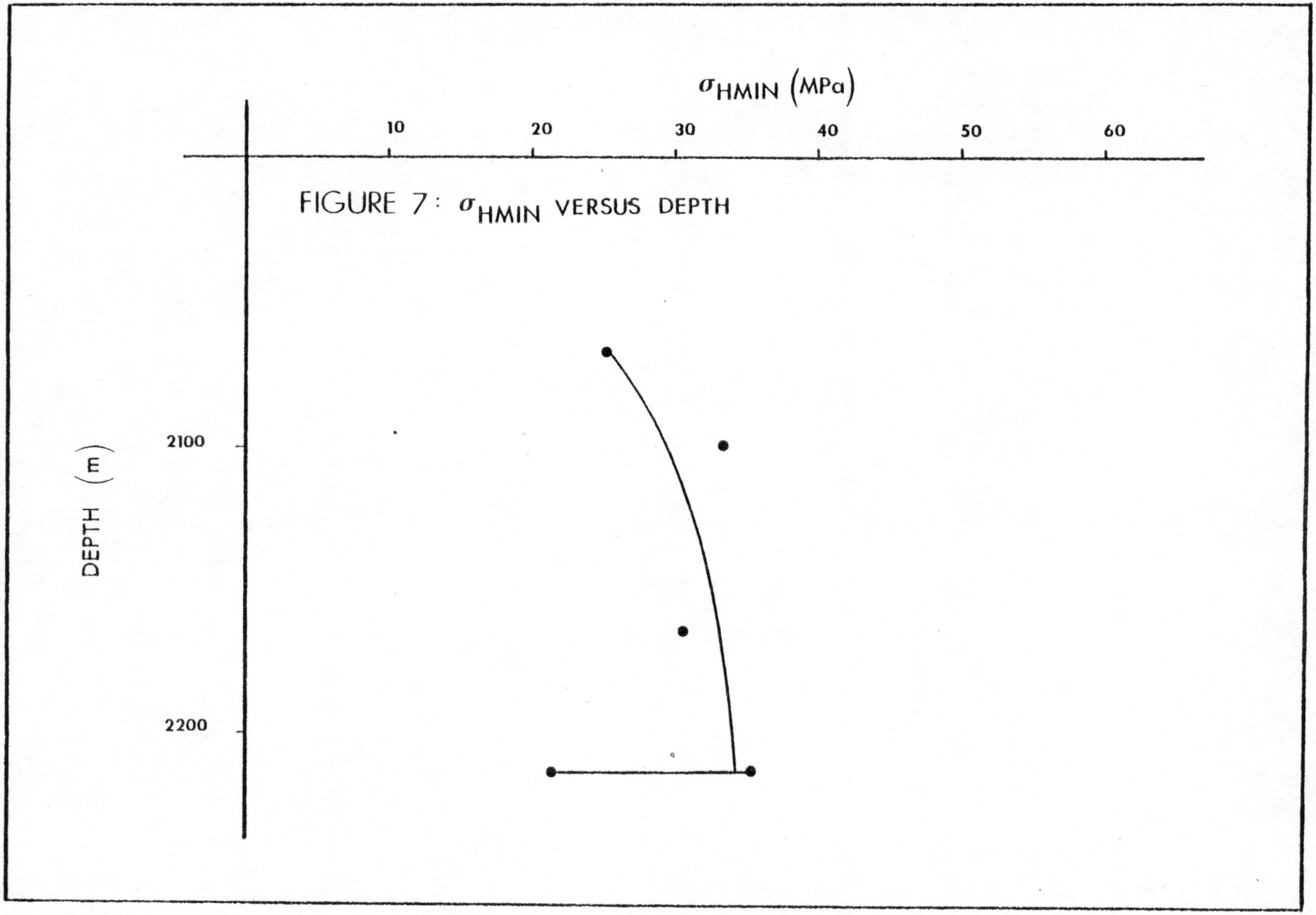

FIGURE 7: σ_{HMIN} VERSUS DEPTH

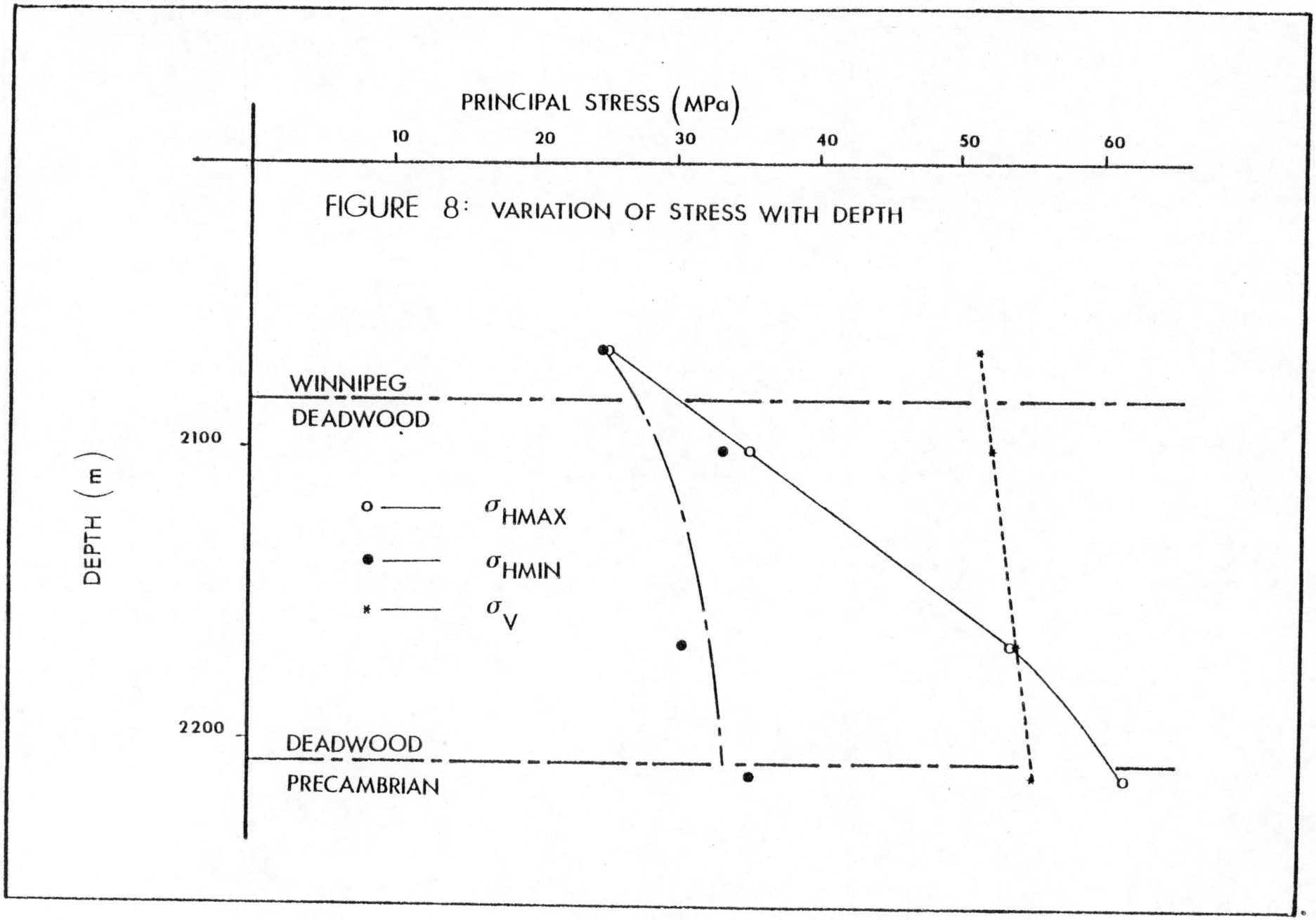

FIGURE 8: VARIATION OF STRESS WITH DEPTH

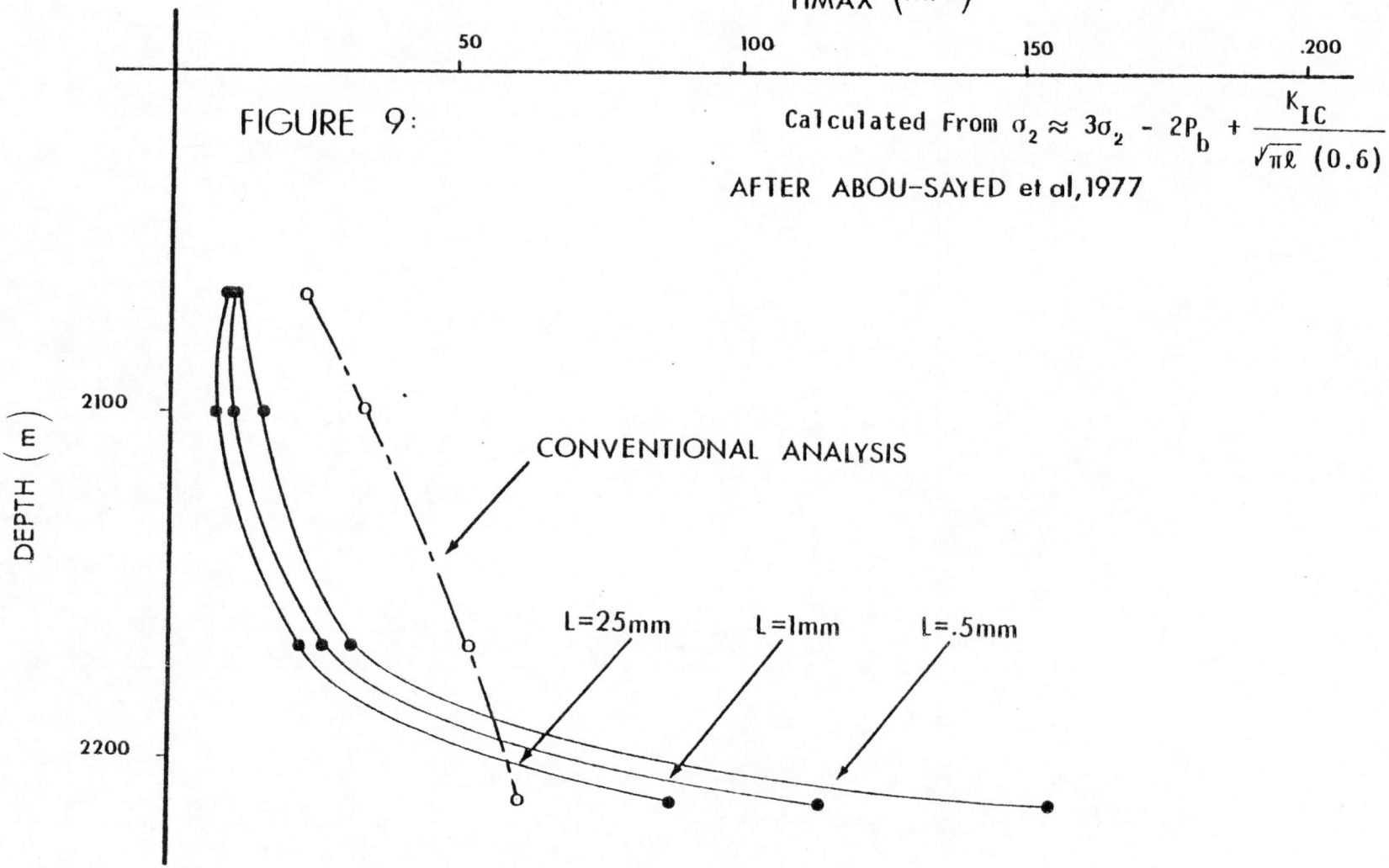

FIGURE 9: Calculated From $\sigma_2 \approx 3\sigma_2 - 2P_b + \frac{K_{IC}}{\sqrt{\pi \ell}\ (0.6)}$

AFTER ABOU-SAYED et al, 1977

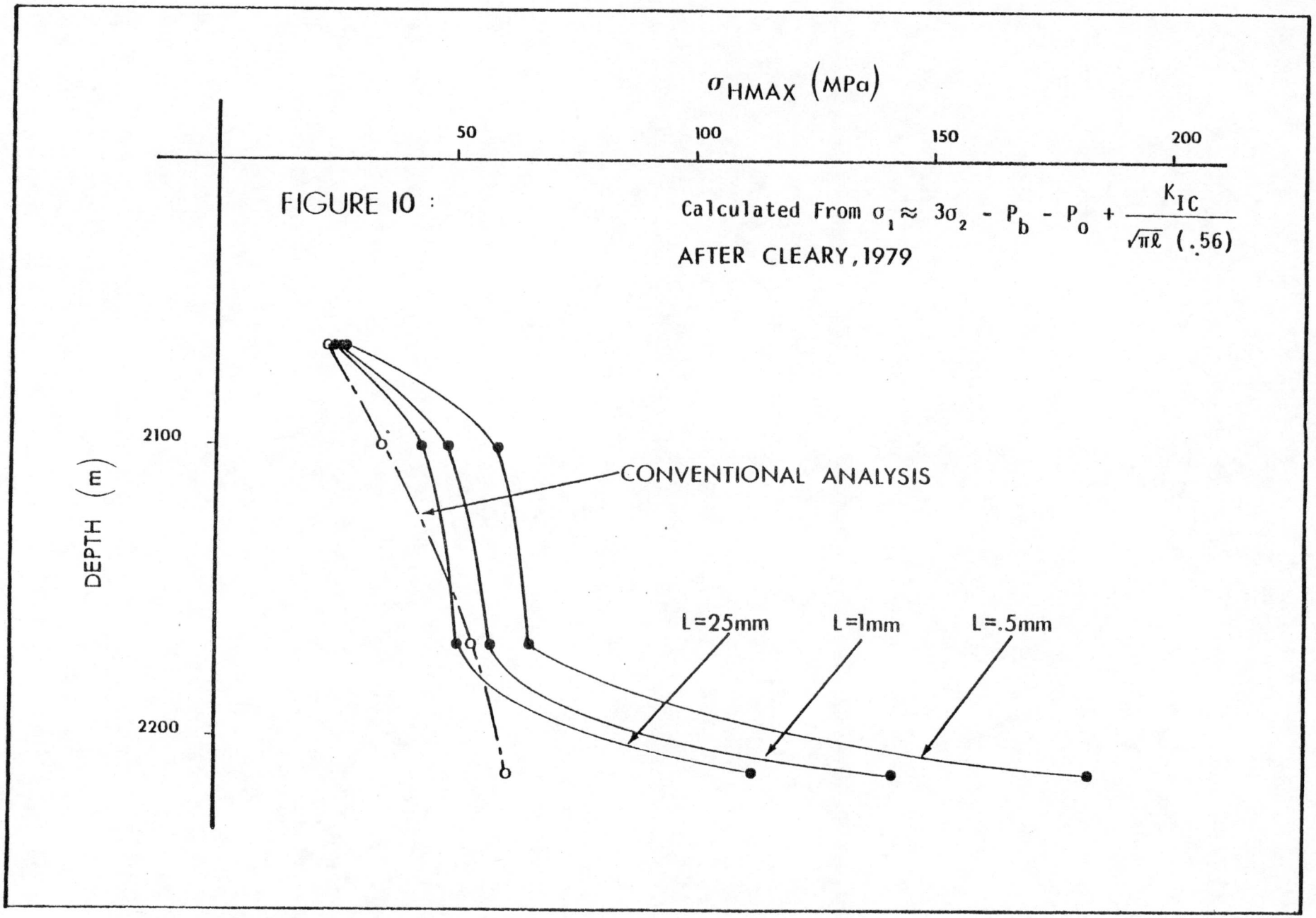

FIGURE 10 : Calculated From $\sigma_1 \approx 3\sigma_2 - P_b - P_o + \frac{K_{IC}}{\sqrt{\pi \ell}\ (.56)}$

AFTER CLEARY, 1979

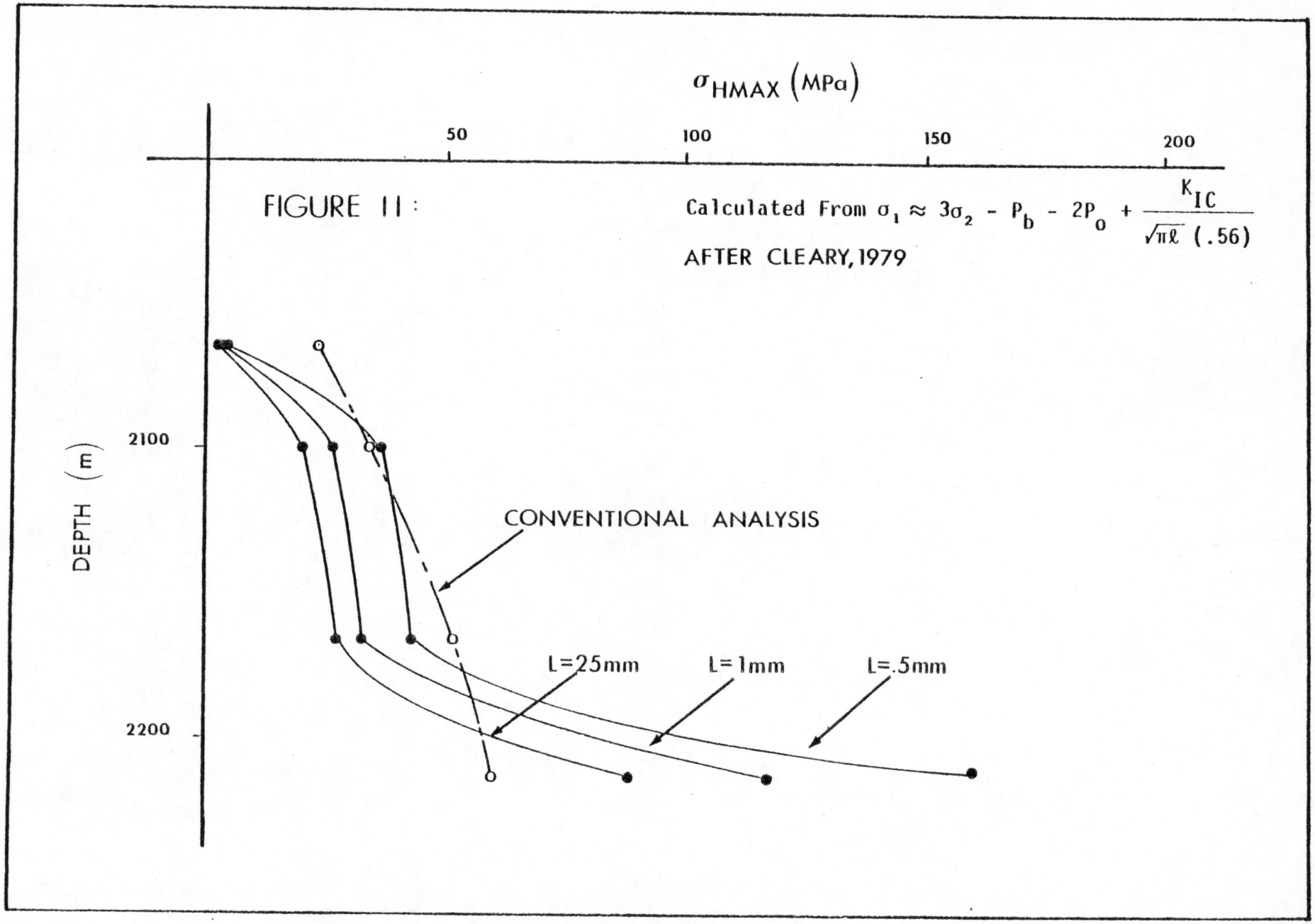

FIGURE 11: Calculated From $\sigma_1 \approx 3\sigma_2 - P_b - 2P_o + \frac{K_{IC}}{\sqrt{\pi \ell}\ (.56)}$

AFTER CLEARY, 1979

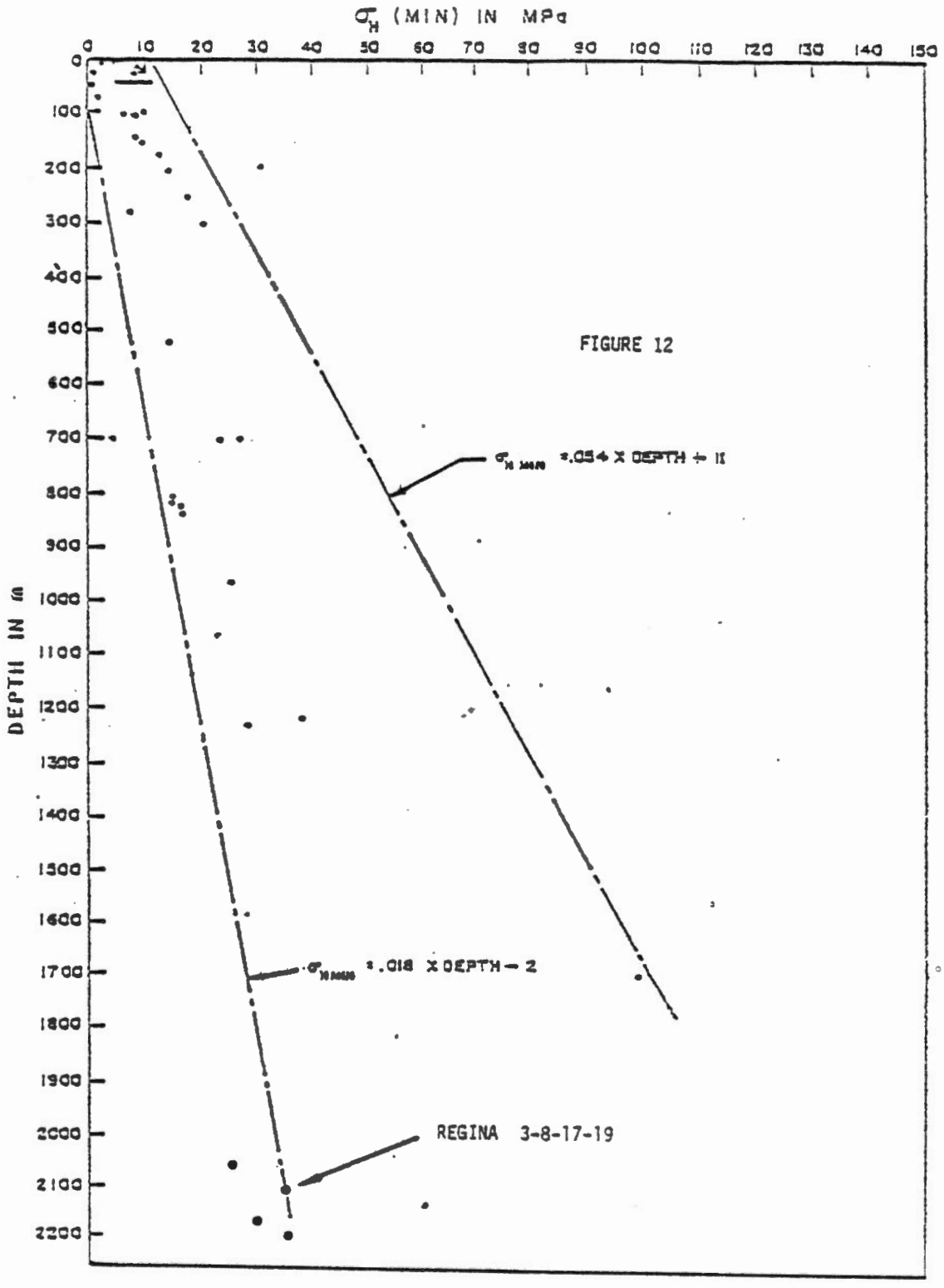

PLOT OF MEASURED VALUES σ_{HMIN} VERSUS DEPTH

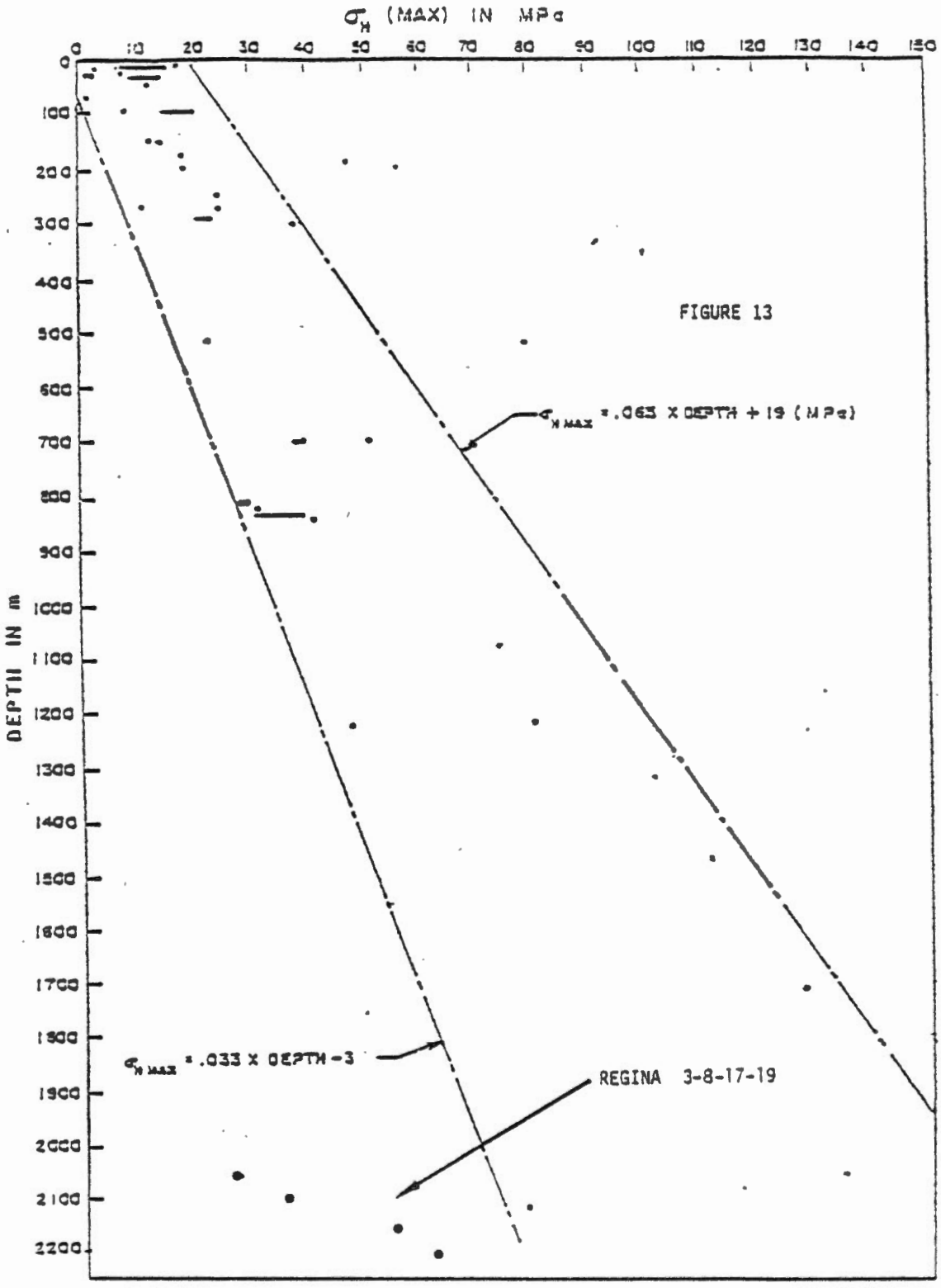

PLOT OF MEASURED VALUES OF σ_{HMAX} VERSUS DEPTH

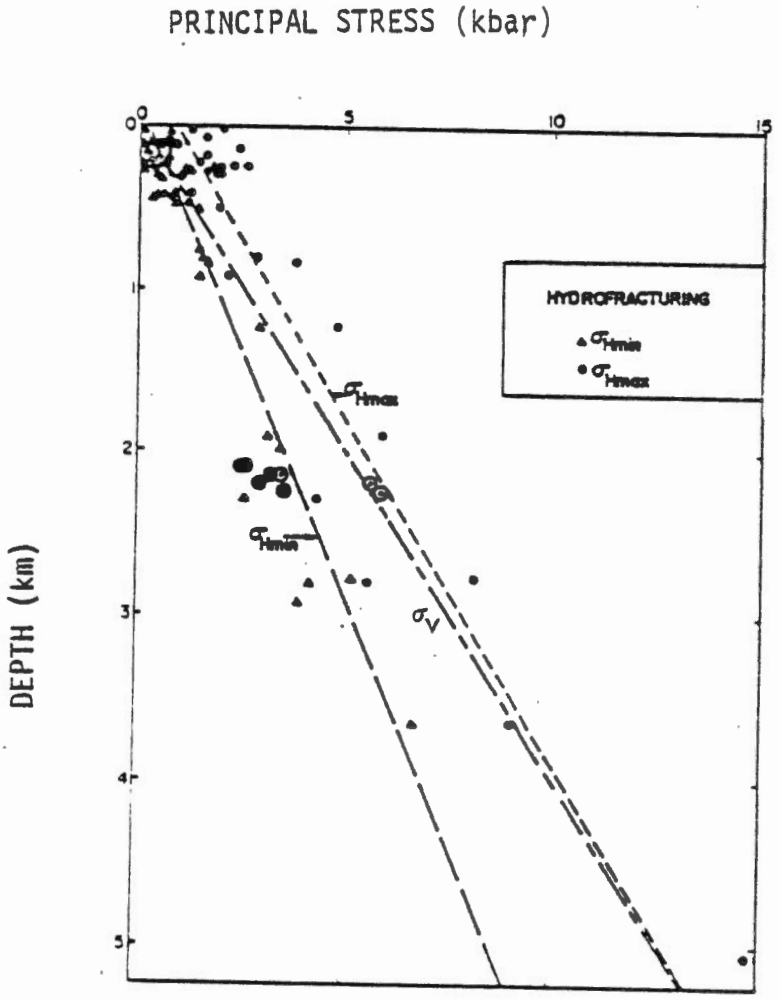

FIGURE 14

VARIATION OF PRINCIPAL STRESS WITH DEPTH

●——— σ_{HMIN}

⊙——— σ_{HMAX}

} REGINA 3-8-17-19

(After Haimson, 1978)

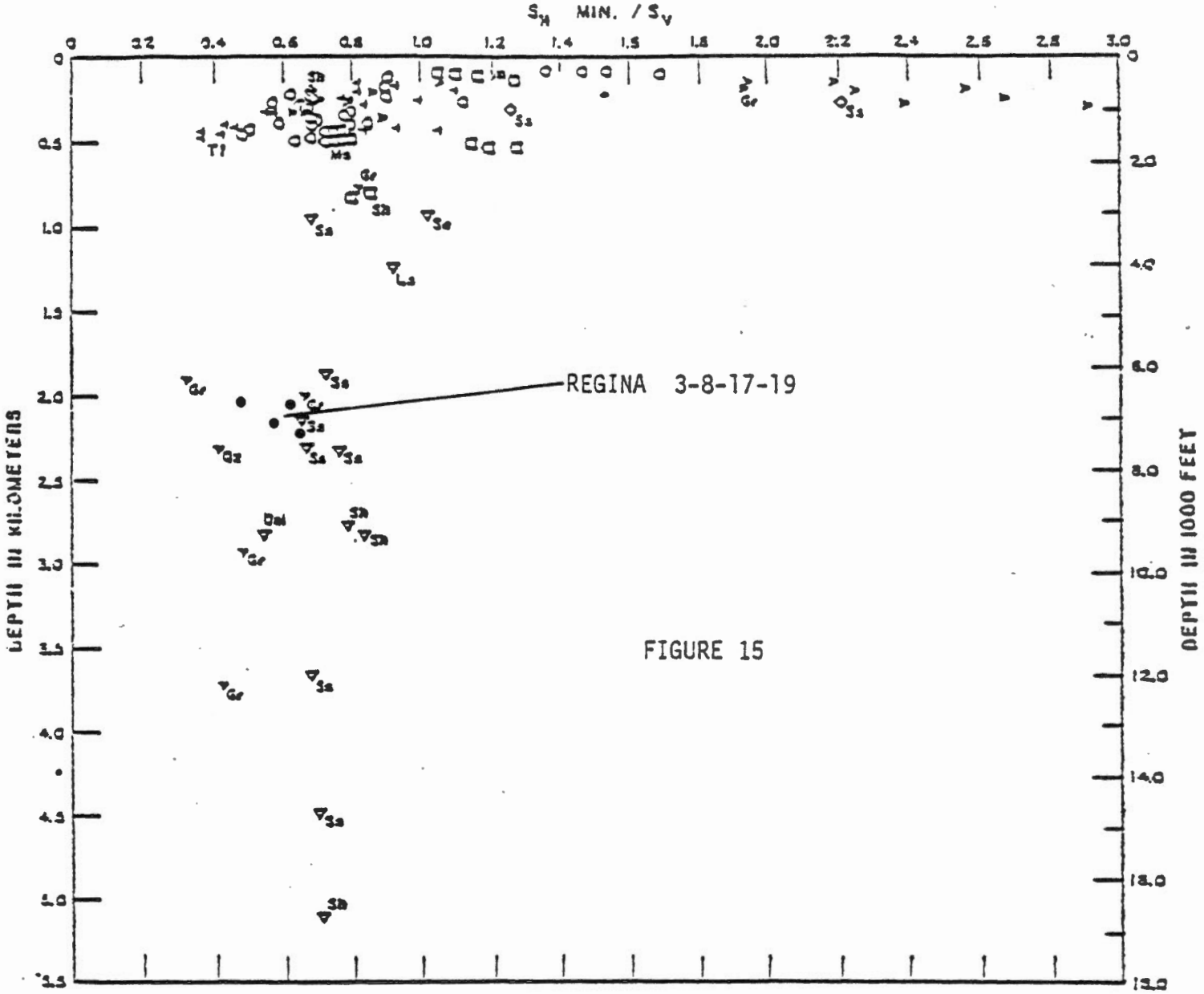

FIGURE 15

LEGEND

ABOVE 600 METERS (2000 FEET)
- PALEOZOIC SEDIMENTS
- TERTIARY SHALE, SANDSTONE (Sh, Ss)
- TERTIARY OIL SHALE (Ms)
- TERTIARY TUFF (T)
- GRANITE, GRANODIORITE, GNEISS

BELOW 600 METERS
- PALEOZOIC SEDIMENTS
- SEDIMENTARY ROCKS
  Se - SALT, Ls - LIMESTONE,
  Ss - SANDSTONE, Dol - DOLOMITE
- CRYSTALLINE, PRE-CAMBRIAN ROCKS
  Qz - QUARTZITE, Gr - GRANITE

Ratio of $\sigma_{H\ min.}$ to σ_{OB} in sedimentary rock (North America)

Reference: Swolfs, H.S., 1977
Abou Sayed, A.S., 1977

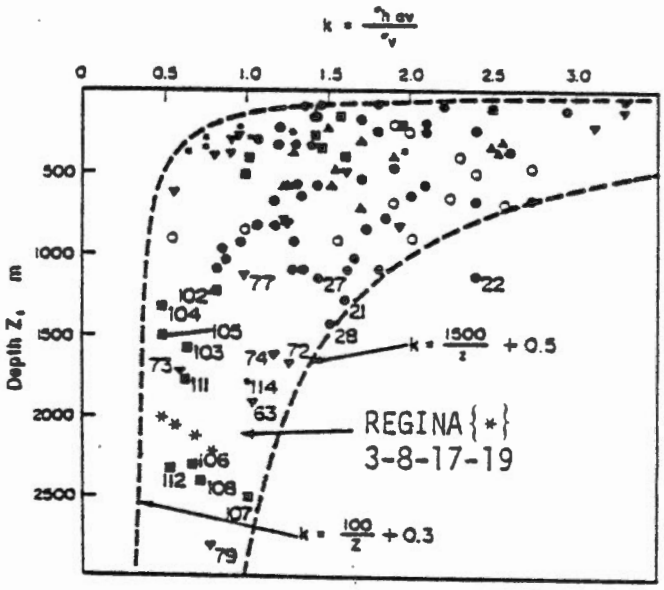

VARIATION OF STRESS RATIO WITH DEPTH
(After Brown & Hoek, 1978)

FIGURE 16

FIGURE 17: ASSORTED DEEP STRESS MEASUREMENTS (DEPTH GREATER THAN 500 METRES) PERFORMED NEAR REGINA

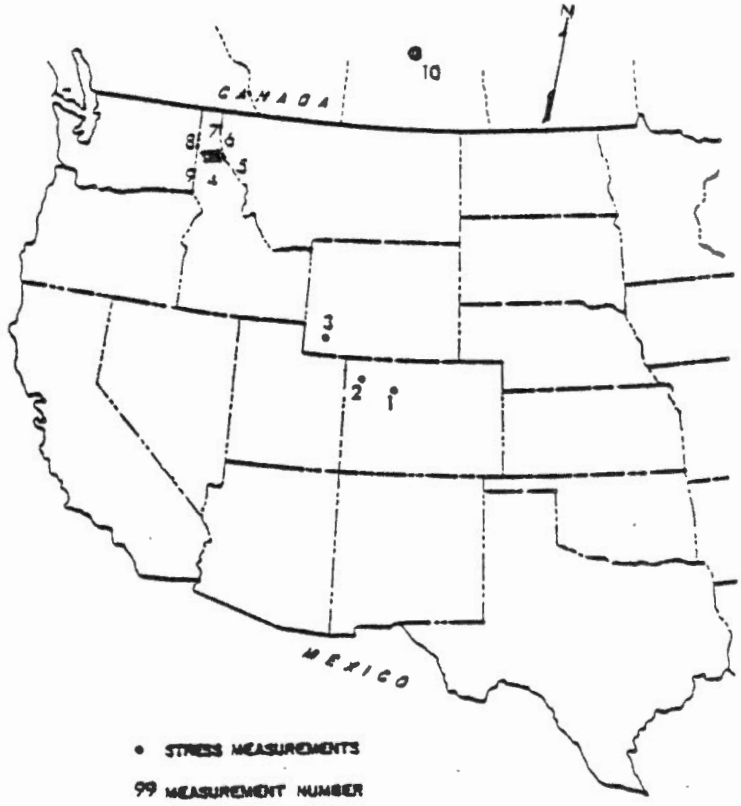

MEASUREMENT NUMBER	TECHNIQUE*1	LOCATION	DEPTH (m)	LITHOLOGY	σ_{HMAX} (MPa)	σ_{HMIN} (MPa)	σ_v (MPa)	DIRECTION OF σ_{HMAX}
1	O	Loveland Pass, Col.	628	Granite	12.20	8.06	18.22	N52°W
			789	or	33.76	27.70	22.53	N23°W
			1135	Ore Body	40.73	25.02	21.97	N39°W
2	H	Rangely, Col.	1912.6-16.3	Sandstone	58.95	31.37	43.44	N70°E
3	O	Green River, Wmg.	488	NA	12.55	6.79	NA	N16°W
4	O	Burke, Idaho	1065	Quartzite	NA	31.0	40.0	NA
			1710	"	NA	40.7	40.0	NA
			2010	"	NA	40.0	38.6	NA
5	O	Coeur d'Alene, Idaho	1220	Quartzite	NA	64.3	36.5	NA
6	O	Osborne, Idaho	1615	Quartzite	51.88	42.27	40.23	N30°W
7	O	Oxburn, Idaho	1671	Quartzite	105.04	37.49	56.74	N25°E
8	O	Coeur d'Alene, Idaho	1585	NA	44.0	25.99	NA	N24°W
9	O	Wallace, Idaho	1220	Quartzite	89.64	48.27	75.35	N45°W
10	H	Regina, Sask.	2065	Sandstone	25.35	25.10	51.40	W20°S
			2100	Sandstone	35.07	33.68	52.27	NA
			2168	Sandstone	53.81	30.62	53.96	N61°W
			2213	Granite	61.71	35.42	55.08	NA

*1 O - OVERCORING
H - HYDRAULIC FRACTURING

*2 ESTIMATED

(After Lindner & Halpern, 1978)

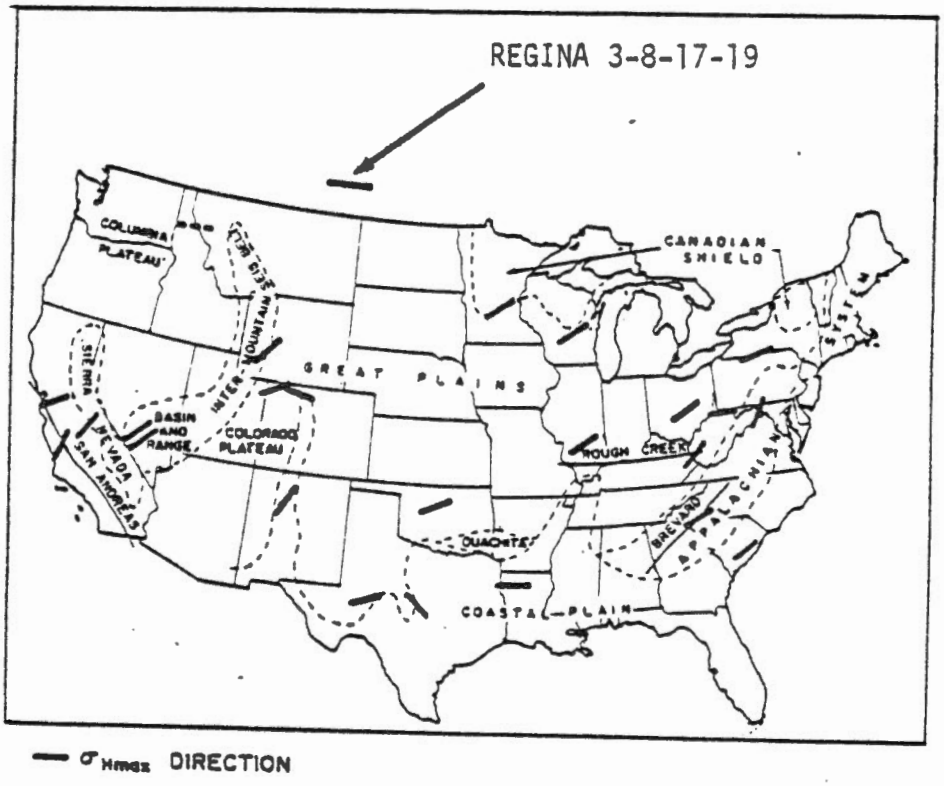

FIGURE 18

(After Haimson, 1978)

AVERAGE DIRECTION OF σ_{HMAX}

APPENDIX A

FRACTURING HISTORY

FRACTURE ONE

Date: May 28, 1979

Depth: 2210.5 - 2215 metres

Fracturing History:

The single packer arrangement was used for this fracture. The tool string was lowered. Bottom was "tagged" and the string was pulled up one metre. The packers were inflated to 8 MPa (measured at the surface). Pumping with the University of Toronto air operated pump could not build pressure higher than about 8.3 MPa.

At this stage, the system was shut-in and Halliburton pumped. At approximately 19 MPa the pressure began to drop off indicating that some form of breakdown, of at least a small-scale nature had occurred. The system was shut-in for several minutes. As soon as repumping started, with no increase in pressure (surface) the formation broke down initially. The system was again shut-in. There was a large degree of oscillation as damping occurred in the drill string.

On repumping, the secondary breakdown peaks were higher. This can happen if:

(a) The fracture encounters some form of obstruction as it propagates radially from the hole.

(b) The fracture encounters a barrier layer.

The latter is quite possibly the case in this situation. Ultimately, flow may have circulated around the packers and eventually reached the annulus through the overlying sandstone.

After several pressurization - shut-in cycles the system was bled off. It is interesting to note the shut-in pressures for the latter cycles did not drop off.

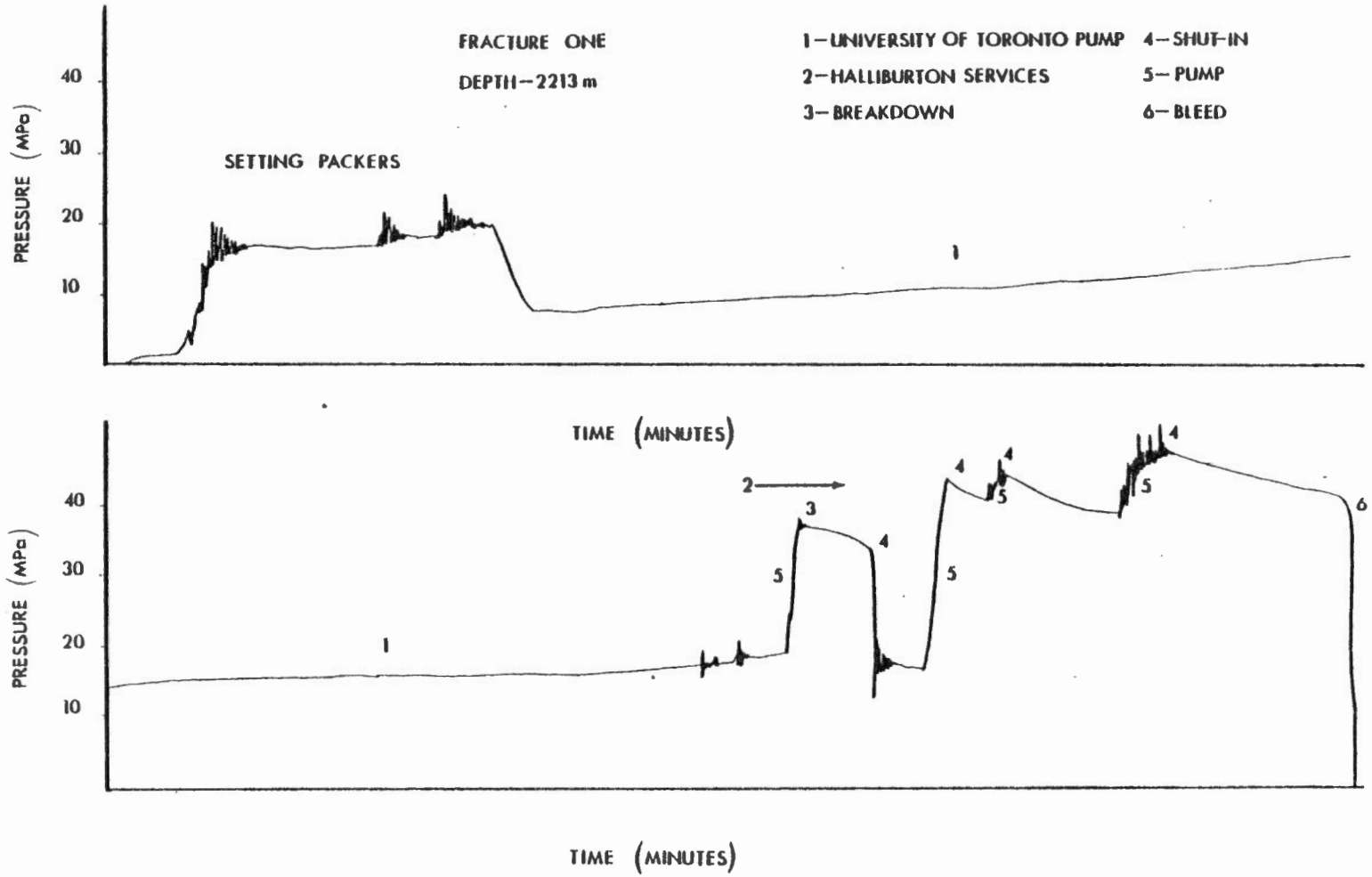
FRACTURE ONE
DEPTH – 2213 m
1 – UNIVERSITY OF TORONTO PUMP
2 – HALLIBURTON SERVICES
3 – BREAKDOWN
4 – SHUT-IN
5 – PUMP
6 – BLEED
SETTING PACKERS
PRESSURE (MPa)
40
30
20
10
TIME (MINUTES)

Critical Pressures:

Pump	Pressure*[1] (MPa)	Flow Rate (US gpm)	Elapsed Time (min)
Halliburton	18.79	.10	1.33
	11.55*[2]	.0	2.33
	5.69*[2]	.0	2.33
	21.55	.10	3.33
	23.10	.10	4.13
	20.34*[3]	.10	4.67
	25.34	.10	6.46

*[1] Pressure measured at the surface

*[2] Instantaneous shut-in pressure

*[3] Small scale additional breakdown during a propagation cycle

FRACTURE TWO

Date: May 30, 1979 and May 31, 1979

Depth: 2167.5 metres to centre of interval

Fracturing History:

The packer arrangement was first installed in the hole on May 30, 1979. On pressurizing the packers, leakage developed and the string was pulled. On May 31, 1979 a new set of packers was attached and pressure tested in the casing. There was no leakage. The tool was lowered to the fracturing interval. The drill string was filled with gel and other additives:

Gel and Additives*

Quantity (lb/1000 gal)	Name	Purpose
20	Adamide Aqua	Reduces spurt losses in the formation by blocking off pores
24	WG11	Gel (increases fluid viscosity)
2	FR20	Reduces friction in drill pipe
10	CW1	Monosodium Phosphate (Water Buffer)

The gel increases the fluid viscosity with essentially no change in density.

The packers were inflated in stages (3.46 MPa, 6.90 MPa, 12.07 MPa). At 12.07 MPa the movements were made and the packers were set. The system was bled off.

---

* Used in all fractures at this site.

Halliburton pumped and there was a breakdown and a well defined shut-in. On repumping the pressure rose much higher and on shutting-in there was no appreciable loss in pressure. With further pumping the pressure increased. With shut-in the pressure held constant temporarily and then dropped drastically, down to the lowest value yet encountered. It was questioned at this stage whether flow was circulating around the packers. To determine this, the annulus between the drill pipe and the borehole wall was filled and on repressurization the annulus pressure was also monitored. On repumping the pressure in the interval (as measured at the surface) rose only slightly. The annulus pressure also rose slightly indicating there was some amount of communication. The system was shut-in. To this stage approximately .89 m^3 had been pumped into the hole. A slug of very viscous gel was next pumped into the hole and at a rate of approximately 1 bbl/min. The volume of the slug was approximately .6 m^3. The character of the very viscous gel was:

Quantity (lb/1000 gel)	Name	Purpose
40	WG11	Gel
2	FR20	Friction reducer
10	CW1	Water buffer
0.5 gal/1000 gal	CL11	Cross-link for drastically increasing the viscosity

With the slug of gel being pushed down the drill tube at approximately 3.8 bbl/min, surface pressure rose rapdily and when pumping stopped pressure dropped down rapidly. On repumping at a rate of

4.3 bbl/min pressure rose rapidly and propagation occurred at a pressure of approximately 22 MPa. On shut-in, the pressure rapidly dropped to approximately 18.98 MPa. The rate of pressure loss temporarily decreased at this point and then dropped rapdily again to approximately 13.11 MPa at which point pressure decreased slowly and regularly. Another pump cycle followed the same sort of pattern. The system was bled off and the test terminated. By the end of the test it was evident that the annulus was being pressurized either through communication through the formation or due to packer failure.

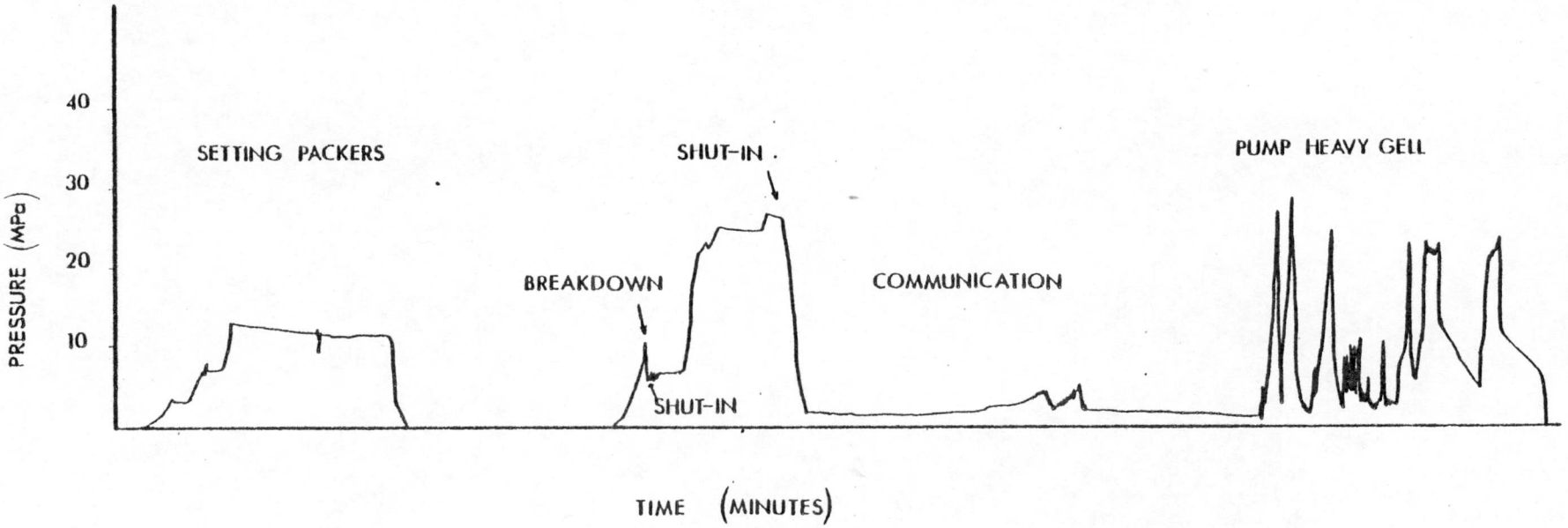

FRACTURE TWO
DEPTH — 2168 m

Critical Pressures:

Pump	Pressure*[1] (MPa)	Flow Rate (US gpm)	Elapsed Time (min)
Halliburton	10.34	10	5.07
	7.24*[2]	0	5.10
	21.38*[3]	10	7.73
	22.76	10	8.03
	22.34*[3]	10	8.27
	24.83	10	8.60
	24.24*[2]	0	8.73
	26.21	10	10.93
	25.66*[2]	0	11.20
	7.24*[4]	0	12.40
	1.72*[5]	0	12.80
	ANNULUS FILLED		12.80 - started 18.47 - completed
Halliburton	4.41	10	21.60
	2.69*[2]	0	21.80
	5.52	10	23.33
	1.79*[2]	0	23.73
	SLUG OF THICK GEL INJECTED		23.73 - started 38.33 - completed
Halliburton	22.76*[3]	180.6	39.60
	12.07*[6]	0	40.27
	12.07*[6]	0	43.13

*[1] Pressure measured at the surface

*[2] Instantaneous shut-in pressure

*[3] Propagation

*[4] Inflection point during shut-in

*[5] Bottom packer has blown

*[6] Packer pressure (approximately)

FRACTURE THREE

Date: June 1, 1979

Depth: 2064 m (centre of interval)

Fracturing History:

Following the "standard" procedure, the packers were set at approximately 11.38 MPa (pressure was raised to this level in stages). The annulus was filled and pumping started with the University of Toronto pump. Pressure could not be built up rapidly enough. Therefore the system was shut-in.

Halliburton began pumping. Pressure rose rapidly. On the first pressurization cycle (pressurizing to 20.52 MPa at a a rate of 0.25 bbl/min) breakdown did not occur. On shut-in, pressure bled off at a slow but moderately steady rate. A similar behaviour was noted on the second pressurization - shut-in cycle (pressure was taken somewhat higher for this cycle). For the third cycle a small amount of propagation occurred at a pressure of approximately 23.79 MPa and shortly afterwards at a pressure of approximately 24.83 MPa.

However, continued pressurization cycles duplicated the previous behaviour to a large extent. On the shut-in portion of the fifth pressurization cycle, there is some indication of closure of a minor fracture at a pressure (surface) of 25.86 MPa.

After this cycle, the entire system was bled off by slowly opening a valve at the surface. The surface line pressure was reduced to approximately 6.38 MPa and was then repressurized. Pressures built up

to approximately the same level. The cyclic behaviour was approximately the same except the shut-in curves were not as smooth indicating that some fracturing may have occurred. For these cycles and for all the other cycles except the first two, there is a relatively small pressure loss during shut-in.

The system was rapidly bled to approximately 2.41 MPa. Pumping commenced again for two pressurization cycles. Behaviour was approximately the same. The system was bled off. On repressurization after this, the slope of the pressurization curve decreased after a pressure of approximately 24.14 MPa. The system was shut-in, repressurized and bled off rapidly several more times. With continued cycling, pressure during shut-in dropped off consistently more rapidly.

Eventually the system was left shut-in for approximately 4.5 minutes. Pressure dropped off to 7.72 MPa. The formation broke down. There was a rapid drop in pressure, eventually levelling out at 1.72 MPa with no further pressure loss.

On repressurization cycles, pressures rose up to former levels. However, there was indication of some form of propagation. Some of the changes in slopes on the pressurization curves are probably due to the rate of pumping into the formation.

During the final pressurization cycle, propagation was evident. 1.5 bbl of fluid were injected into the borehole with no appreciable increase in pressure. On shut-in for this cycle, pressure decreased in a uniform fashion to 16.21 MPa after which point pressure decayed at a considerably smaller rate.

The system was bled off and the packers were deflated.

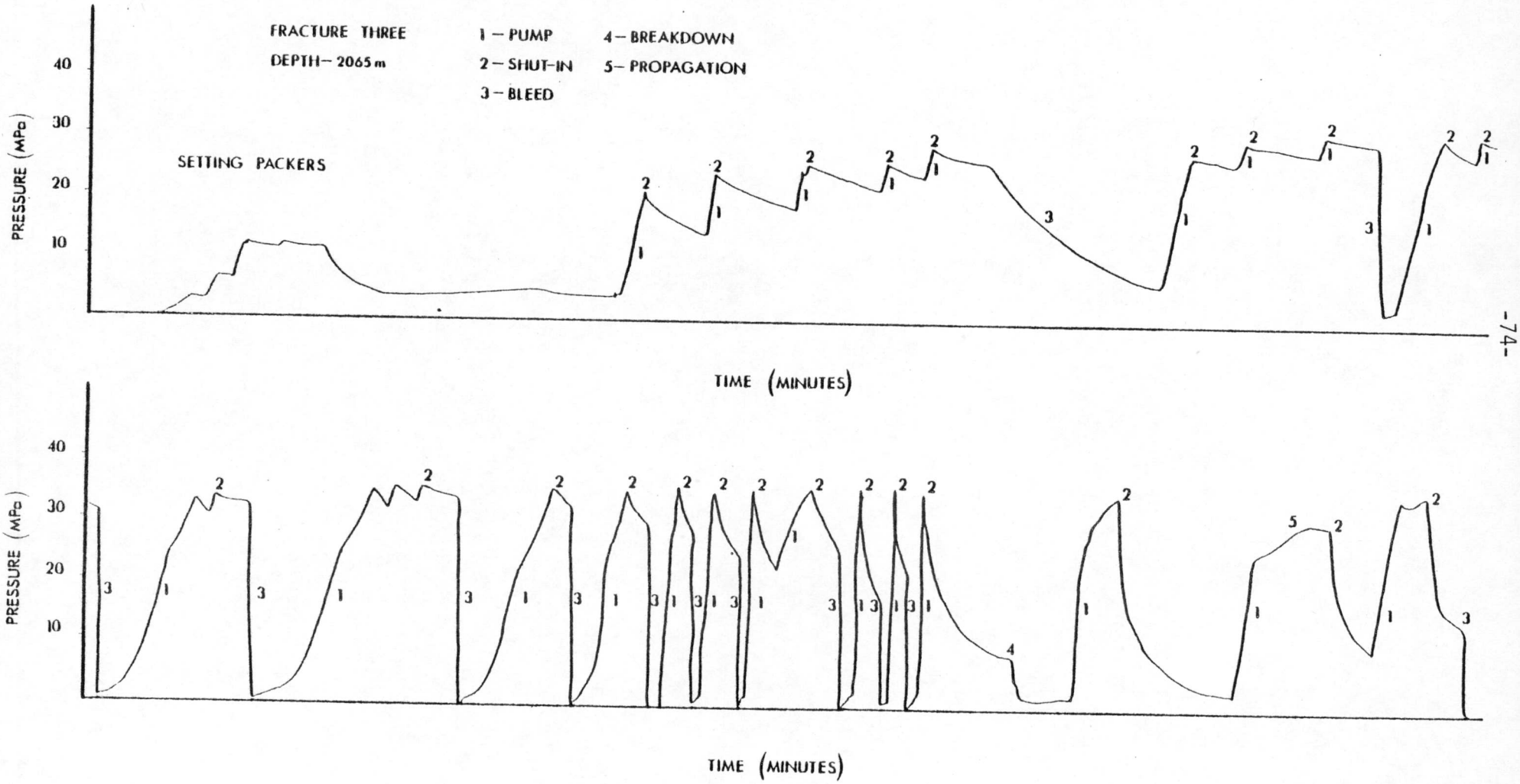
FRACTURE THREE
DEPTH– 2065 m
1 – PUMP
2 – SHUT-IN
3 – BLEED
4 – BREAKDOWN
5 – PROPAGATION
SETTING PACKERS
PRESSURE (MPa)
40
30
20
10
TIME (MINUTES)
PRESSURE (MPa)
40
30
20
10
TIME (MINUTES)

Critical Pressures:

Pump	Pressure*[1] (MPa)	Flow Rate (US gpm)	Elapsed Time (min)
Halliburton			started at 10.8 min
	20.41	10	12
	24.14	10	15.4
	24.62*[3]	10	19.3
	25.52*[3]	10	19.6
	25.86	10	22.7
	28.10	10	24.8
	25.86*[3]	10	26.9
	BLEED SLOWLY TO 6.41 MPa		
	27.93	10	37.0
	30.00	10	39.5
	31.55	10	43.3
	BLEED RAPIDLY TO 2.41 MPa		
	31.31	10	48.8
	31.31	10	50.7
	BLEED RAPIDLY TO 0 MPa		
	24.14*[4]	10	55.4
	32.59	10	56.6
	33.45	10	57.4
	BLEED RAPIDLY TO 0 MPa		
	24.14*[4]	10	63.5
	34.83	10	64.7
	35.17	10	65.9
	35.17	10	67.2
	BLEED RAPIDLY TO 0 MPa		
	22.41*[4]	10	71.8
	26.90*[4]	10	72.5
	34.83	10	73.3
	BLEED RAPIDLY TO 0 MPa		
	25.52*[4]	10	76.0
	35.00	10	76.8
	BLEED RAPIDLY TO 0 MPa		
	35.00	10	78.7
	BLEED RAPIDLY TO 0 MPa		
	35.17	10	80.5
	BLEED RAPIDLY TO 0 MPa		
	35.31	10	82.3
	35.17	10	85.1

Critical Pressures:

Pump	Pressure*1 (MPa)	Flow Rate (US gpm)	Elapsed Time (min)
	BLEED RAPIDLY TO 0 MPa		
	35.17	10	87.4
	BLEED RAPIDLY TO 0 MPa		
	35.17	10	89.0
	BLEED RAPIDLY TO 0 MPa		
	34.31	10	90.3
	7.59	0	94.6
	1.72*2	0	95.2
	33.03	10	99.5
	24.83	70	105.9
	29.66	70	108.6
	33.79	70	113.1
	34.48	70	114.3
	16.90*2	0	115
	7.24	BLEEDING	116.2

*1 Surface pressure (MPa)

*2 Instantaneous shut-in pressure

*3 Anomalous behaviour while the system is shut-in

*4 Change in slope of pressurization curve

FRACTURE FOUR

Date: June 1, 1979

Depth: 2071 m (centre of interval)

Fracturing History:

The packers were set and the annulus filled. The system was pumped to approximately 27.59 MPa (surface) and shut-in. Pressure decreased only slightly. Pressure was increased and shut-in again with negligible pressure decay. With a further increase in pressure, there was detectable pressure decay during the shut-in.

The pressurization loop was bled and repressurized. On shut-in, pressure again dropped off slightly. The pressurization shut-in cycle was repeated. On the final pressurization cycle pressure did not decay during shut-in.

The formation did not break down. This interval was abandoned.

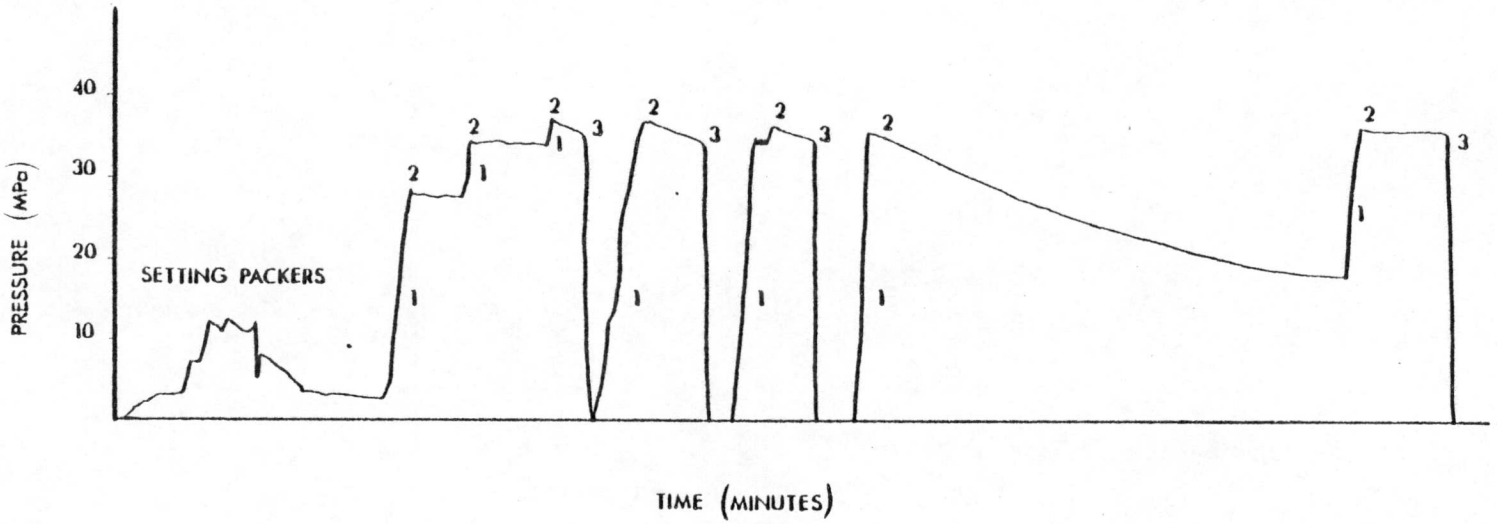

FRACTURE FOUR

DEPTH – 2071 m

1 – PUMPING

2 – SHUT-IN

3 – BLEED

Critical Pressures:

Pump	Pressure*1 (MPa)	Flow Rate (US gpm)	Elapsed Time (min)
Halliburton	28.62	10	.8
	35.02	10	3.5
	34.14*2	0	3.6
	37.24	10	6.1
	BLEED RAPIDLY TO 0 MPa		
	37.24	10	9.3
	BLEED RAPIDLY TO 0 MPa		
	36.21	10	13.6
	BLEED RAPIDLY TO 0 MPa		
	36.72	10	17.3
	36.55	0	35.3
	35.52	10	34.9

*1 Surface Pressure (MPa)

*2 Instantaneous Shut-in Pressure

FRACTURE FIVE

Date: June 1, 1979

Depth: 2100 m (centre of interval)

Fracturing History:

The packers were set at 11.72 MPa. Pressure was being built up. At a surface pressure of 28.97 MPa pressure dropped rapidly to 11.03 MPa and bled off slowly after this.

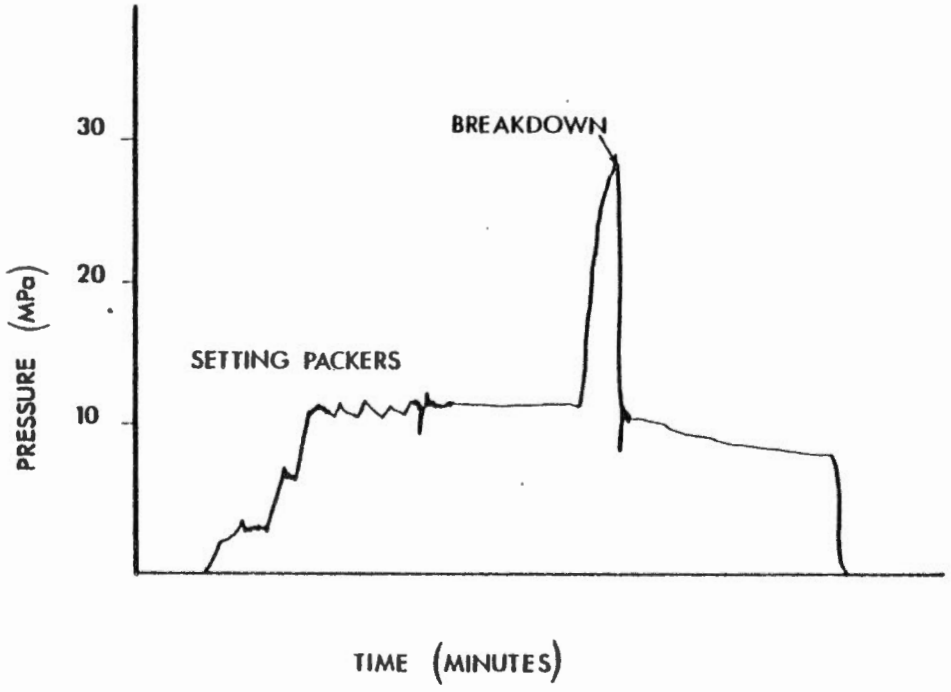

FRACTURE FIVE

DEPTH – 2100 m

Critical Pressures:

Pump	Pressure*[1] (MPa)	Flow Rate (US gpm)	Elapsed Time (min)
Halliburton	28.97	10	.7
	11.03	0	.8

*[1] Pressure measured at the surface.

APPENDIX B

DOWNHOLE PRESSURE-TIME RECORDS

DOWNHOLE PRESSURE-TIME RECORD
FRACTURE ONE DEPTH - 2213 m

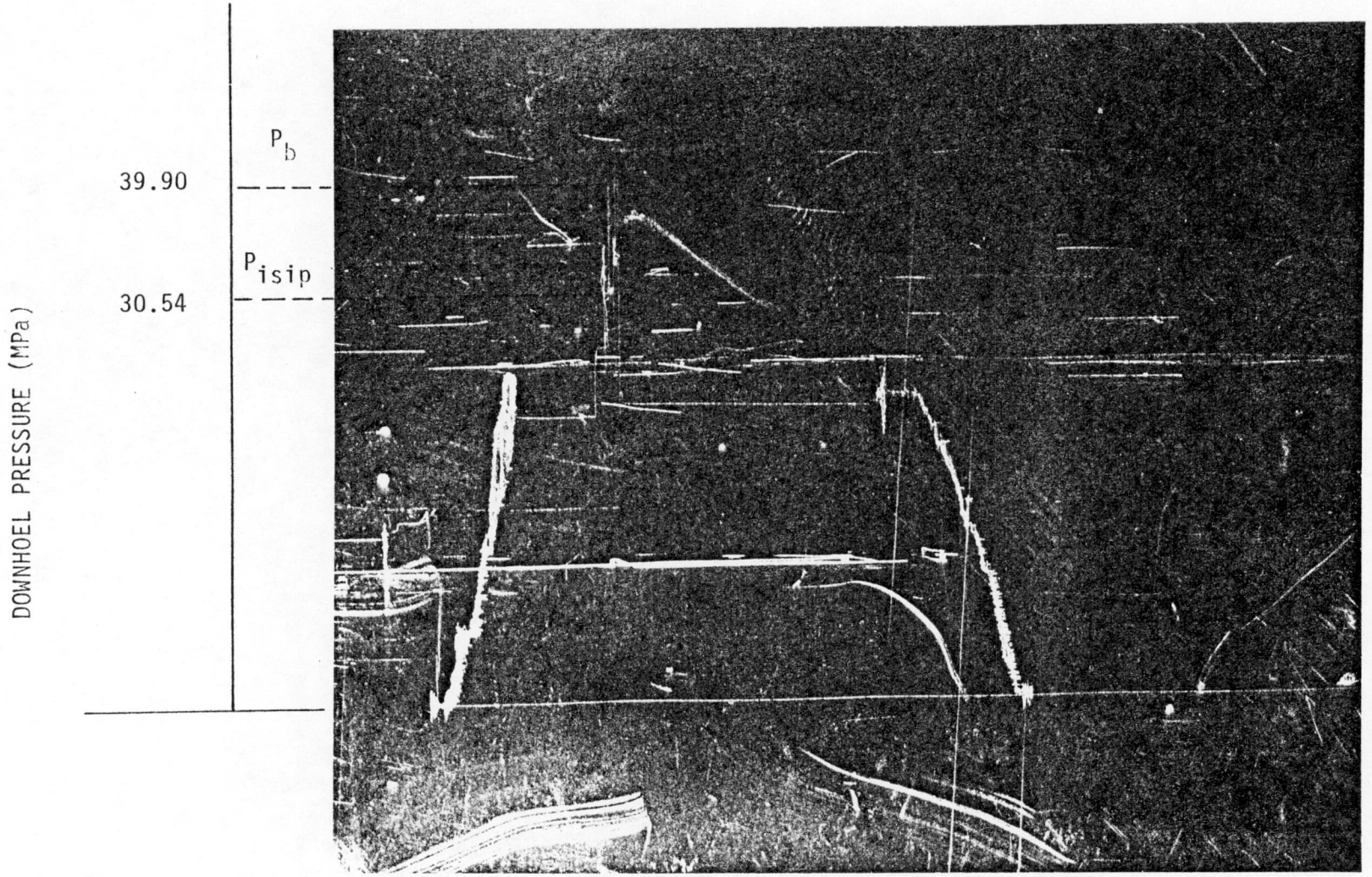

DOWNHOLE PRESSURE-TIME RECORD

FRACTURE TWO DEPTH - 2168 m

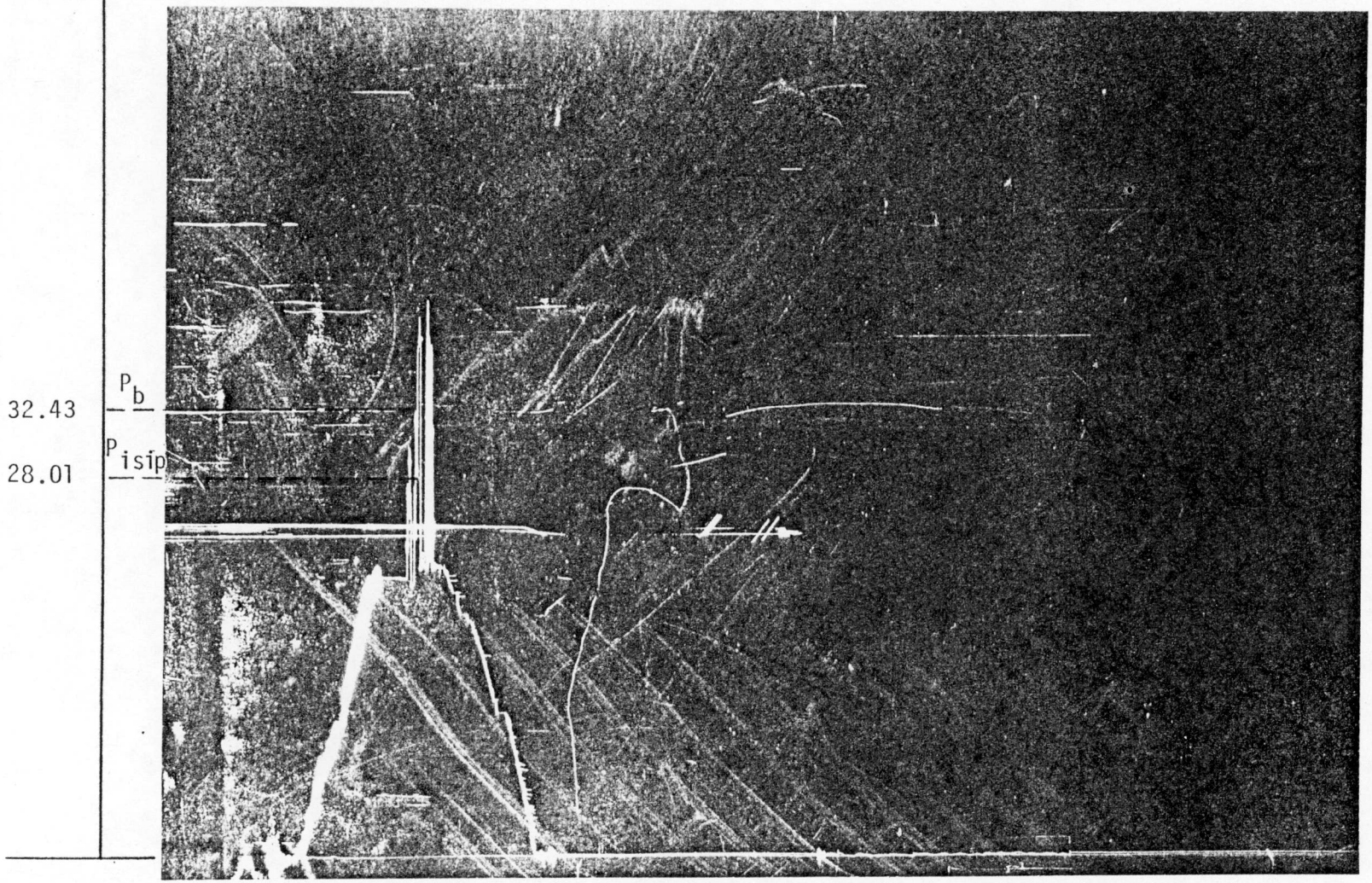

DOWNHOLE PRESSURE-TIME RECORD

FRACTURE DEPTH - m

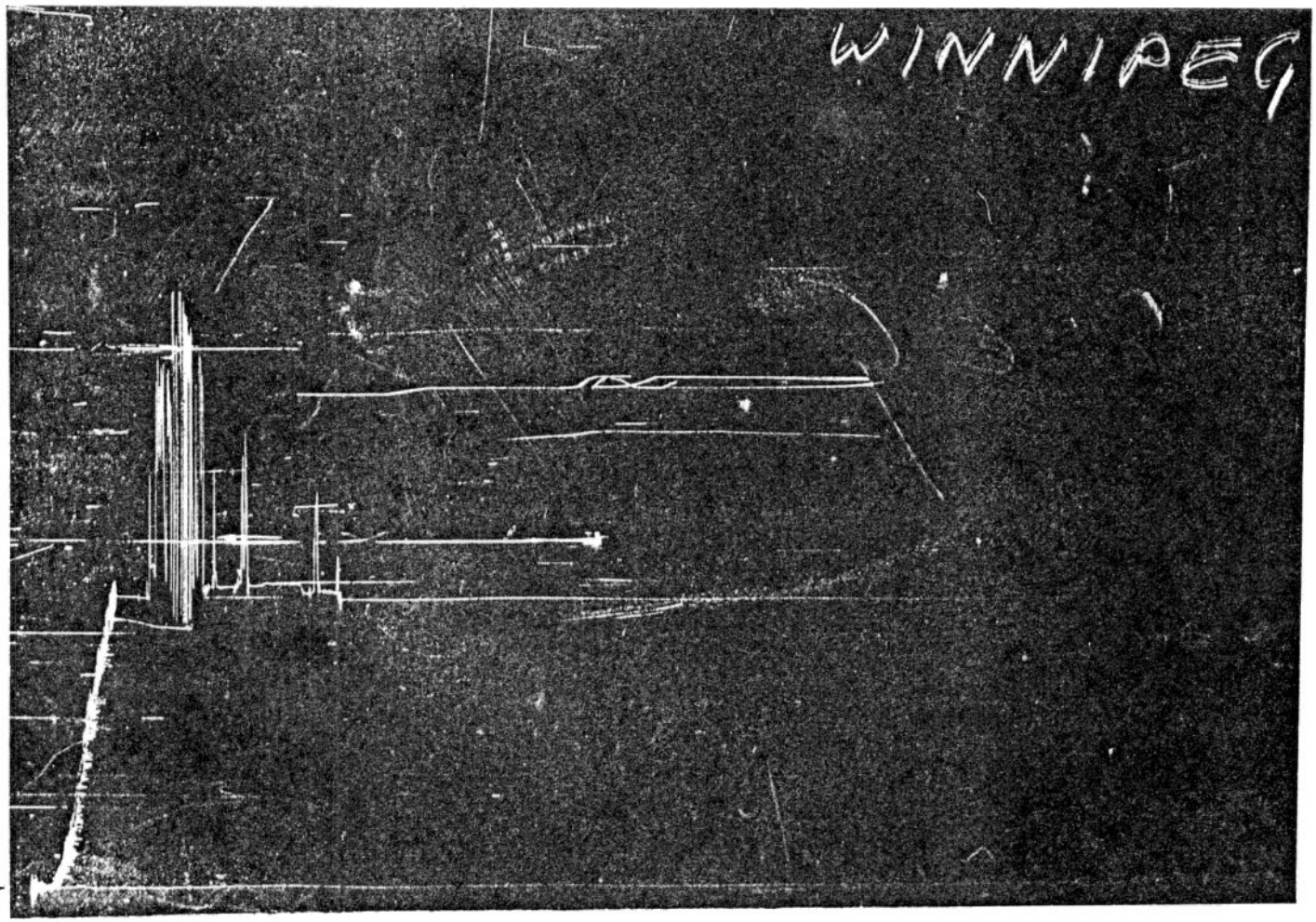

DOWNHOLE PRESSURE (MPa)

APPENDIX C

APPLICATION OF FRACTURE MECHANICS CONCEPTS TO HYDRAULIC FRACTURING ANALYSIS

PART A

MODE I CONDITIONS

(C.1) GENERALITIES

Hardy, 1973, discussed fracture mechanics considerations applicable to hydraulic fracturing.. His treatment can be briefly synthesized as follows.

Consider a fracture geometry as shown in Figure A, this being after initiation of a fracture from a pressurized borehole.

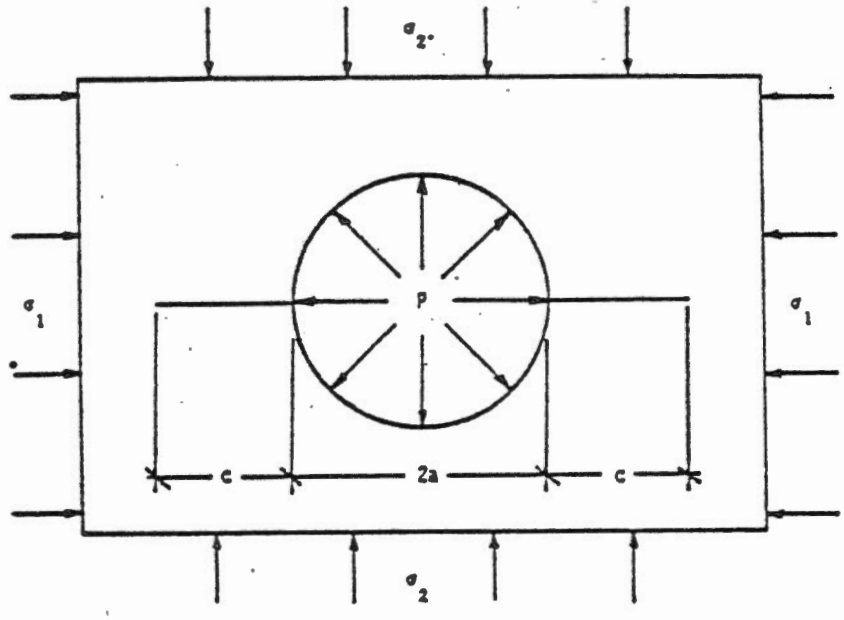

PRESSURIZED BOREHOLE (CRACKED) WITH STRESSES σ_1, σ_2 ACTING AT INFINITY

FIGURE A

Two parameters f(c/a) and g(c/a) have been defined by Cottrell in 1972.

$$f(c/a) = \frac{GE}{q^2 \pi a} \tag{C-1}$$

$$g(c/a) = \frac{GE}{p^2 \pi a} \tag{C-2}$$

where:

G – strain energy release rate

E – Young's Modulus

q – Tensile stress perpendicular to the crack

p – Compressive stress parallel to the crack

a – Borehole radius

c – Crack length

Hardy, 1973, states that for a tensile stress $(p-\sigma_2)$ perpendicular to the crack, the opening mode stress intensity factor is:

$$K_I\ (p-\sigma_2) = (p-\sigma_2)\ \left[\ \pi a f\left(\frac{c}{a}\right)\right]^{\frac{1}{2}} \tag{C-3}$$

For a compressive stress (σ_1-p) parallel to the crack, the opening mode stress intensity factor is:

$$K_I\ (\sigma_1-p) = (\sigma_1-p)\left[\pi a g\left(\frac{c}{a}\right)\right]^{\frac{1}{2}} \tag{C-4}$$

By superposition,

$$K_I = (p-\sigma_2)\left[\pi a f\left(\frac{c}{a}\right)\ \right]^{\frac{1}{2}} + (\sigma_1-p)\left[\pi a g\left(\frac{c}{a}\right)\right]^{\frac{1}{2}} \tag{C-5}$$

Hardy states that at crack extension $K_I = (\gamma E)^{\frac{1}{2}}$. This would seem to be appropriate only under plane stress conditions. In general, as has been shown, for a MODE I situation:

$$G_{ICR} = \frac{\pi\ (\kappa+1)\ k_1^2}{8\mu} \tag{C-6}$$

where:

$$k_1 = K_I/\sqrt{\pi} \tag{C-7}$$

Extension can allegedly occur when

$$G_{ICR} > \gamma \tag{C-8}$$

Under plane stress

$$G_{ICR} = \frac{\pi\ (\frac{3-\nu}{1+\nu} + \frac{1+\nu}{1+\nu})\ k_1^2}{8\ \frac{E}{2(1+\nu)}} \tag{C-9}$$

$$= \frac{k_1^2\ \pi\ (\frac{4}{1+\nu})}{\frac{4}{1+\nu}\ E} = \frac{k_1^2\ \pi}{E} \tag{C-10}$$

At failure

$$k_1^2 = \frac{\gamma E}{\pi} \tag{C-11}$$

$$k_1 = \sqrt{\frac{\gamma E}{\pi}} \tag{C-12}$$

$$K_I = \sqrt{\gamma E} \tag{C-13}$$

However, if the situation is plane strain:

$$G_{ICR} = \frac{\pi\ (3-4\nu+1)\ k_i^2}{8\ \frac{E}{2(1+\nu)}} \tag{C-14}$$

$$= \frac{4\pi\ (1-\nu)\ k_1^2}{4\ \frac{E}{1+\nu}} = \frac{\pi\ (1-\nu)^2\ k_1^2}{E} \tag{C-15}$$

This implies that extension will occur for

$$k_1^2 = \frac{\gamma E}{\pi(1-\nu^2)} \tag{C-16}$$

or,

$$K_I = \left(\frac{\gamma E}{1-\nu^2}\right)^{\frac{1}{2}} \tag{C-17}$$

Consider $K_I = \left(\frac{\gamma E}{1-\nu^2}\right)^{\frac{1}{2}}$, p at crack extension would be:

$$p = \frac{\left[\frac{\gamma E}{\pi a(1-\nu^2)}\right]^{\frac{1}{2}} + \sigma_2\left[f\left(\frac{c}{a}\right)\right]^{\frac{1}{2}} - \sigma_1\left[g\left(\frac{c}{a}\right)\right]^{\frac{1}{2}}}{\left[f\left(\frac{c}{a}\right)\right]^{\frac{1}{2}} - \left[g\left(\frac{c}{a}\right)\right]^{\frac{1}{2}}} \tag{C-18}$$

p can be determined uniquely as a function of crack length.

$$\text{For } \sigma_1 = \sigma_2 = 0\ ;\quad \sigma_t = \frac{\left[\frac{\gamma E}{\pi a(1-\nu^2)}\right]^{\frac{1}{2}}}{\left[f\left(\frac{c}{a}\right)\right]^{\frac{1}{2}} - \left[g\left(\frac{c}{a}\right)\right]^{\frac{1}{2}}} \tag{C-19}$$

(σ_t - tensile strength of the rock)

For $\sigma_1 = \sigma_2$

$$P = \frac{\left[\frac{\gamma E}{\pi a(1-\nu^2)}\right]^{\frac{1}{2}}}{\left[f\left(\frac{c}{a}\right)\right]^{\frac{1}{2}} - \left[g\left(\frac{c}{a}\right)\right]^{\frac{1}{2}}} + \sigma_1 \qquad (C-20)$$

as compared to conventional predictions:

$$P = \sigma_t + 2\sigma_1 \qquad (C-21)$$

If hydraulic fracturing were attempted in a region with a pre-existing crack or joint along the axis of the borehole, across the fault $\sigma_t = 0$ and $\gamma = 0$. An apparent discrepancy now arises since:

from (C-19) $p = \sigma_1$ (C-22)

from (C-20) $p = 2\sigma_1$ (C-23)

Hardy states that if the pressure at which flow from the borehole into the joint were recorded, and if this pressure were used as a measure of the stress state around the borehole, equation (C-22) should be used.

For some ratios of σ_1/σ_2 there may be a size effect on the breakdown pressure, expressed as:

$$p^* = f\,(\sigma_1, \sigma_2, c/a, c, E, \gamma)$$
$$\searrow \qquad (C-24)$$
$$p\cdot(\pi a(1-\nu^2)/E\gamma)$$

If σ_1/σ_2 is large and is constant and if the value of c is stationary on the (c/a) curve, then there will be a reduction in p_b for increases in the internal hole diameter.

(C.2) NO FLUID PENETRATION INTO AN EXISTING FRACTURE

If there is no penetration, this is analogous to having an impermeable membrane in the borehole. Oucherlony (1972) (Refer to Figure B) has considered such a situation:

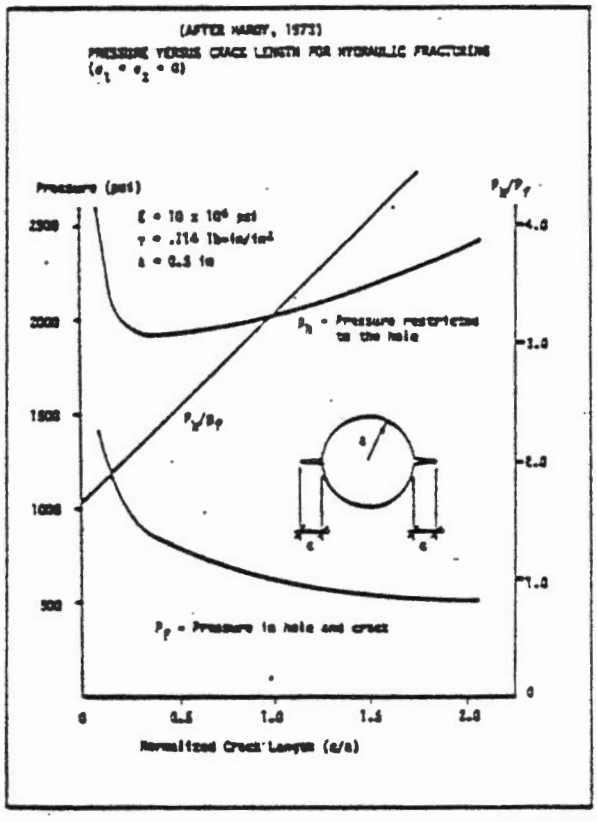

FIGURE B

For no penetration:

$$K_I = p(\pi a)^{\frac{1}{2}} F(c/a) \qquad (C\text{-}25)$$

For σ_1 parallel to the crack:

$$K_I = \sigma_1 \left[\pi a g(c/a)\right]^{\frac{1}{2}} \tag{C-26}$$

For σ_2 perpendicular to the crack:

$$K_I = -\sigma_2 \left[\pi a f(c/a)\right]^{\frac{1}{2}} \tag{C-27}$$

Using superposition,

$$K_I = p(\pi a)^{\frac{1}{2}} F(c/a) - \sigma_2 \left[\pi a f(c/a)\right]^{\frac{1}{2}} + \sigma_1 \left[\pi a g(c/a)\right]^{\frac{1}{2}} \tag{C-28}$$

with,

$$K_I = \left[\frac{E\gamma}{(1-\nu^2)}\right]^{\frac{1}{2}} = (E')^{\frac{1}{2}}$$

$$P = \frac{(E')^{\frac{1}{2}} + \sigma_2 \left[f(c/a)\right]^{\frac{1}{2}} - \sigma_1 \left[g(c/a)\right]^{\frac{1}{2}}}{F(c/a)} \tag{C-29}$$

$$\text{if } \sigma_1 = \sigma_2 = 0 \longrightarrow P = (E')^{\frac{1}{2}}/F(c/a) \tag{C-30}$$

$$\text{if } \sigma_1 = \sigma_2 \longrightarrow P = \frac{(E')^{\frac{1}{2}}}{F(c/a)} + \frac{\sigma_1 \left[f(c/a)^{\frac{1}{2}} - g(c/a)\right]^{\frac{1}{2}}}{F(c/a)} \tag{C-31}$$

(C-31) indicates that for large crack lengths, the breakdown pressure increases very rapidly with increasing crack length.

(* NO PENETRATION).

For a preexisting fracture intersecting the hole

$$p = \frac{\sigma_1 \left[f(c/a)^{\frac{1}{2}} - g(c/a) \right]^{\frac{1}{2}}}{F(c/a)} \qquad (C\text{-}32)$$

For small initial crack lengths (4-32) reduces to:

$$p = 2\sigma_1 \qquad (C\text{-}33)$$

(C.3) FLUID PENETRATION

Hardy considered a purely mode I situation. Zoback et al also did. However, they considered fluid penetration into diametrically opposed pressurized cracks. The pressure distribution was considered uniform throughout the fracture length.

For two fractures stemming from a circular hole in an infinite medium, Newman calculated the normalized stress intensity factors (K_I/p) as a function of crack length ℓ (using geometry shown in Figure C)

$\lambda = 0$ fluid pressure applied only to the borehole

$\lambda = 1$ fluid pressure applied over the fracture surface as well.

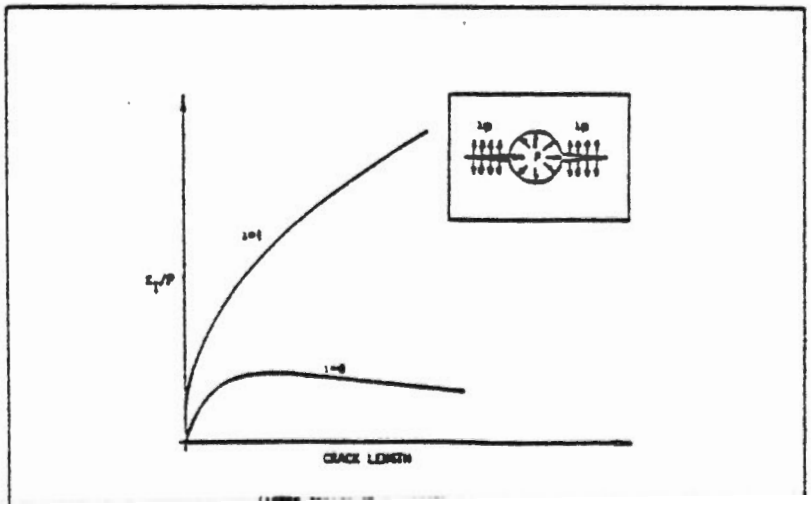

FIGURE C

If the fluid pressure is acting along the entire fracture surface, the stress intensity factor grows as the fracture extends and unstable crack growth would be consequent. When fluid acts only in the borehole, after an initially unstable growth, the stress intensity slowly decreases with crack length (stable crack growth - requires increasing pressure for continued crack propagation). The reality lies somewhere between these two limits.

(C.4) VERTICAL FRACTURE MIGRATION

Abou Sayed et al, 1977 analyse a vertically migrating hydraulic fracture. (If higher order terms are omitted this is still mode I analysis). An elliptical crack is considered. The crack is subjected to fluid pressure acting on the crack faces and a far-field in situ stress (both varying linearly with depth).

The problem considered is one of quasistatic crack extension, neglecting fluid flow, for a three dimensional crack configuration.

Let:

$\beta = \rho g$ (ρ - fluid density, g - gravitational acceleration)

α = vertical gradient of horizontal insitu stress.

Stress intensity factors, theoretically derived, vary around the crack periphery in a manner implying that an elliptical crack subjected to the prescribed loads will not grow uniformly, even if subjected to uniform pressure. For uniform pressure, the analysis predicts that an elliptical crack will grow into a circular one.

In addition, for nonuniform loading, a circular crack will tend to extend first at the tip which lies on the major axis and $\phi = 0$ (Refer to Figure D).

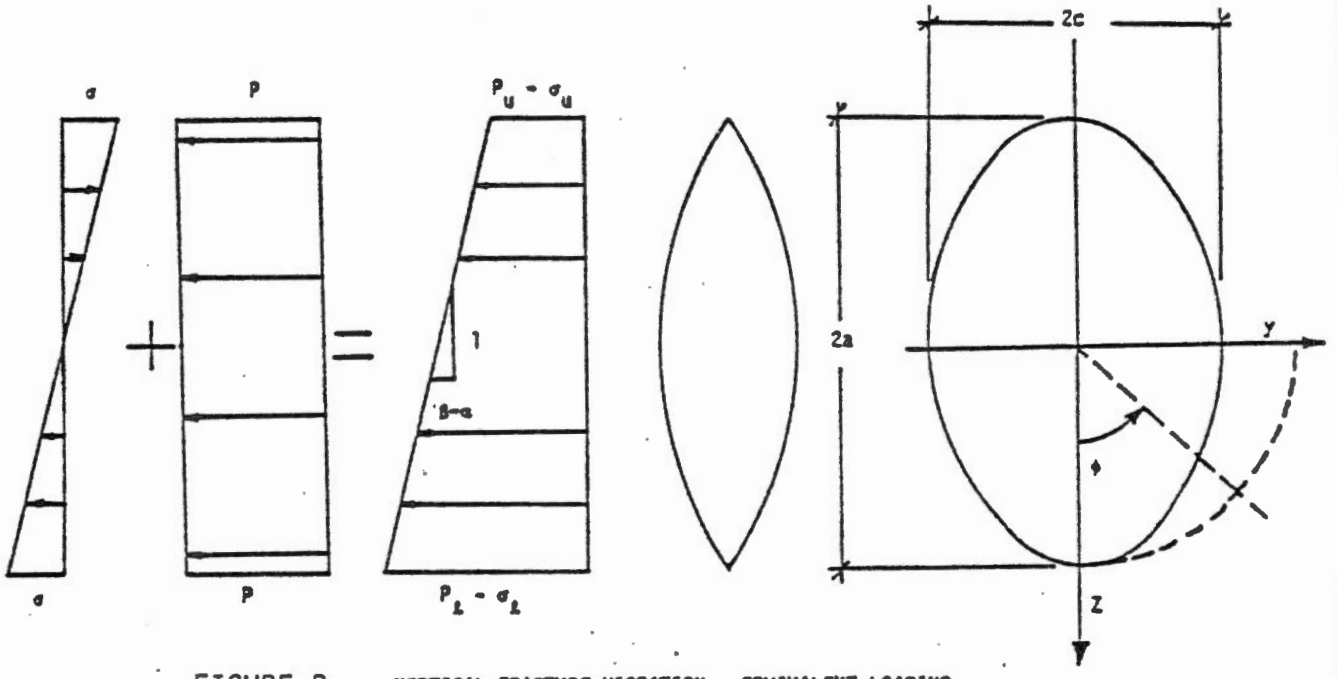

FIGURE D VERTICAL FRACTURE MIGRATION: EQUIVALENT LOADING OF THE ELLIPTICAL FRACTURE (AFTER ABOU-SAYED ET AL, 1977)

$$P = \frac{1}{2}(P_u + P_L) - (\sigma_u + \sigma_L)$$

$$\sigma = \frac{1}{2}(P_L - P_u) + (\sigma_L + \sigma_u) = (\beta - \alpha)\, a$$

"That is, for a downward fracturing condition, a circular crack will tend to become longer in the vertical direction than in the horizontal direction at its lower half, i.e. c/a will tend to decrease. Once this growth has occurred, the new crack will take an intermediate shape between a circle and an ellipse."

Abou Sayed et al, 1977.

(C.5) PARTICULAR FIELD CONDITIONS

"Hydraulic fracture containment is discussed from the point of view of linear elastic fracture mechanics. Three cases are analysed: a) Effect of different material properties for the pay zone and the barrier formation, b) Characteristic of fracture propagation into region of varying in-situ stress and, c) Effect of hydrostatic

pressure gradients on fracture propagation into overlying or underlying barrier formations. The analysis shows the importance of the elastic properties, the in-situ stresses and the pressure gradients on fracture containment."

Simonson et al, 1977.

"1. Hydraulic fractures in a pay zone located between two adjacent barrier layers will tend to be contained provided the stiffness of the pay zone is less than the stiffness of the barrier layers. Furthermore, if the opposite condition exists, barrier penetration is most likely.

2. Migration of a hydraulic fracture either upward or downward in an isotropic, homogeneous medium may be controlled by the density of the hydarulic fracture fluid. If the fluid density gradient is greater (less) than the in-situ stress gradient downward (upward) migration is most probable.

3. If there exists a difference in in-situ stress between the barrier layer and the pay zone with greater in-situ stress in the barrier layer, then it may be possible to detect fracture propagation into the barrier formation. A sudden increase in pumping pressure will occur as the fracture crosses the interface and extends into the barrier layer. The increase in pressure is a function of the difference in in-situ stress between the barrier and pay zone layers and the height of the pay zone."

Simonson et al, 1977.

(C.6) PENETRATION OF A VISCOUS FLUID

Zoback and Pollard, 1978, considered fluid penetration using more realistic assumptions of distribution and character of fluid.

"In attempting to intuitively understand the fracture initiation and extension process, it is necessary to consider the coupled problem of the elastic deformation of a fracture and viscous fluid flow into it. The necessity of considering this coupled problem is illustrated by the extreme cases shown in Figure E ."

Zoback and Pollard, 1978.

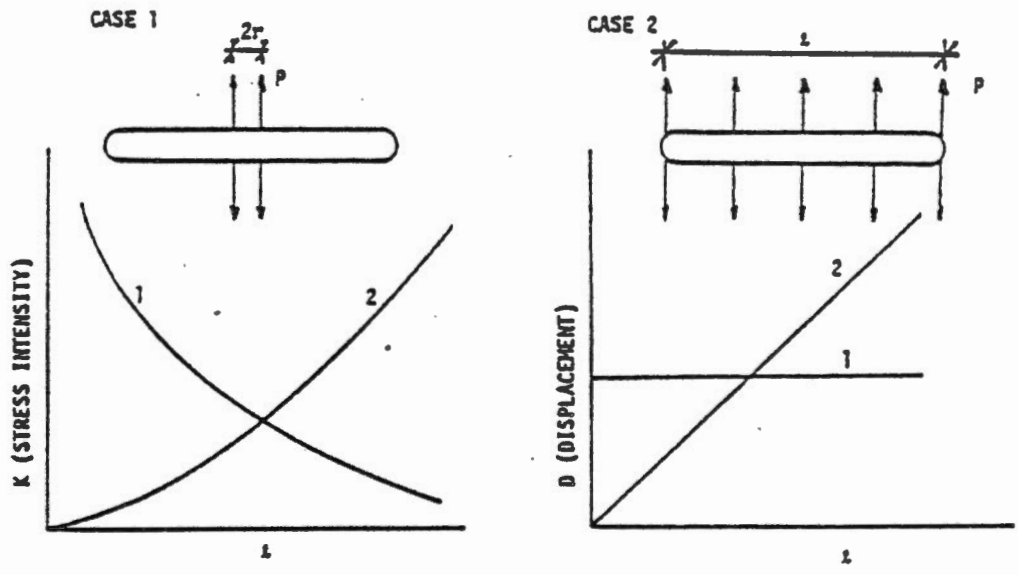

(AFTER ZOBACK & POLLARD, 1978)

SCHEMATIC REPRESENTATION OF STRESS INTENSITY FACTOR AND DISPLACEMENT, AS A FUNCTION OF CRACK LENGTH, FOR TWO LOADING CASES.

FIGURE E

These authors consider:

$$\text{(CASE 1)} \quad \left.\begin{aligned} K &= 2Pr\sqrt{1/2\,\ell\pi} \\ D &= 2Pr\,(1-\nu)\left[1-(2x/\ell)^2\right]^{1/2}/\pi G \end{aligned}\right\} \qquad \text{(C-34)}$$

$$\text{(CASE 2)} \quad \left.\begin{aligned} K &= P\sqrt{\ell\pi} \\ D &= P\,(1-\nu)\left[1-(2x/\ell)^2\right]^{1/2}/2G \end{aligned}\right\} \qquad \text{(C-35)}$$

where:

K – Opening mode stress intensity factor

P – Uniform Pressure

2r – Interval of pressurization for Case One

ℓ – Fracture length

D – Opening displacement of Fracture Wall

ν – Poisson's Ratio

G – Shear Modulus

A propogating fracture cannot be represented precisely by either of these extreme models. Fluid pressure may act in the fracture to some degree, but not necessarily such that fracture propagation is unstable at all times.

Zoback and Pollard utilize a two-dimensional plane strain fracture model in an infinite continuum which is linear elastic, homogeneous, and isotropic. Also considered is steady, constant property flow of a Newtonian viscous fluid "into" the fracture from the borehole. It is assumed that the fracture propagates perpendicular to the least principal compressive stress. Shear stresses on the fracture face due to fluid flow are ignored.

Also considered, using a one dimensional steady state flow law is the crack-tip stress intensity factor as a function of the fracture half-length for various fluid viscosities. Figure F summarizes their findings. This figure, along with Figure G seem to be a good approach. The problem seems to lie with what must be regarded as seeming intuitively unlikely. This is that (Refer to Figure G) wall displacement is herein predicted to increase with decreasing viscosity. The likelihood of this is suspect.

PART B

MIXED MODE CONDITIONS

(C.7) THE EFFECT OF PREFERRED CRACK ORIENTATION ON HYDRAULIC FRACTURING CRACK GROWTH

Consider an existing pressurized crack randomly oriented with respect to the principal stresses (Figure H). Abou Sayed et al, 1977, outline conditions and characteristics of additional propagation.

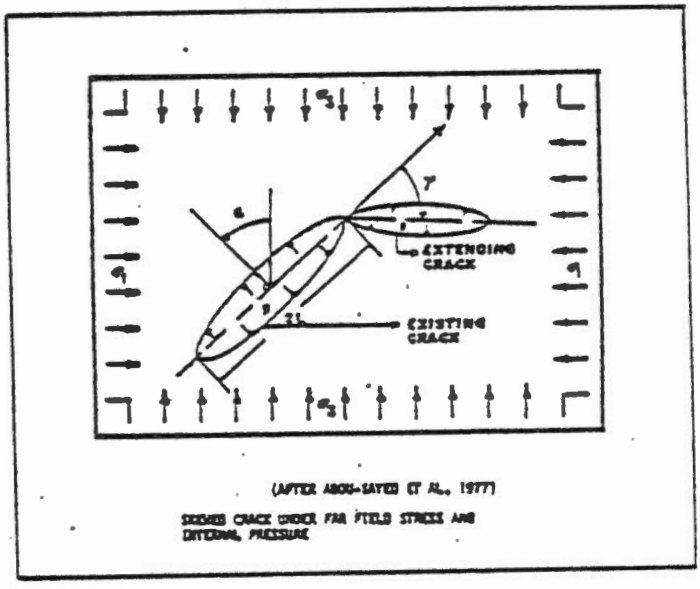

FIGURE H

For the situation shown in Figure H

$$K_I = \sqrt{\pi L}\left[p - \sigma_1 \sin^2\alpha - \sigma_3 \cos^2\alpha\right] \qquad (C\text{-}36)$$

$$K_{II} = \sqrt{\pi L}\left[1/2\,(\sigma_1 - \sigma_3)\sin 2\alpha\right] \qquad (C\text{-}37)$$

These are the stress intensity factors for the existing crack.

If the existing crack extends in an arbitrary direction

$$G(\gamma) = \frac{4(1-\nu^2)}{E}\left(\frac{1}{3+\cos^2\gamma}\right)\left(\frac{\pi-\gamma}{\pi+\gamma}\right)^{\gamma/\pi}\left\{(1+3\cos^2\gamma)\,K_I^{\,2} + 8\sin\gamma\cos\gamma\,K_I\,K_{II} + (9-5\cos^2\gamma)\,K_{II}^{\,2}\right\} \qquad (C\text{-}38)$$

$G(\gamma)$ — strain energy release rate as a function of the angle of extension measured clockwise with respect to the trace of the existing crack.

K_I, K_{II} — given in (C-36) and (C-37)

(after Hussain, et al, 1973, modified for plane strain).

For an open, stationary long crack, a prerequisite is $K_I = K_{II} = 0$. (These considerations seem dubious since it implies that a crack is unstable if $G(\gamma) \neq 0$. Propagation only occurs when $G(\gamma)$ exceeds a characteristic value $G_{CR}(\gamma)$).

$$P = \sigma_1 \sin^2\alpha + \sigma_3 \cos^2\alpha \qquad \text{(C-39)}$$

and

$$(\sigma_1 - \sigma_3) \sin 2\alpha = 0 \qquad \text{(C-40)}$$

For $\sigma_1 \neq \sigma_3$: $\alpha = 0$ or $\alpha = \pi/2$. This implies that the existing crack is stationary if it is parallel to principal stress directions and if the pressure p is equal to the principal stress acting perpendicularly to the crack face. Further considerations indicate extension will tend to be perpendicular to the direction of minimum compressive stress as expected.

A consequence is that σ_3 is equal to the shut-in pressure and if α is known, σ_1 can be evaluated.

(C.8) CRACK INITIATION WITH A PRE-EXISTING CRACK OF PRESCRIBED ORIENTATION

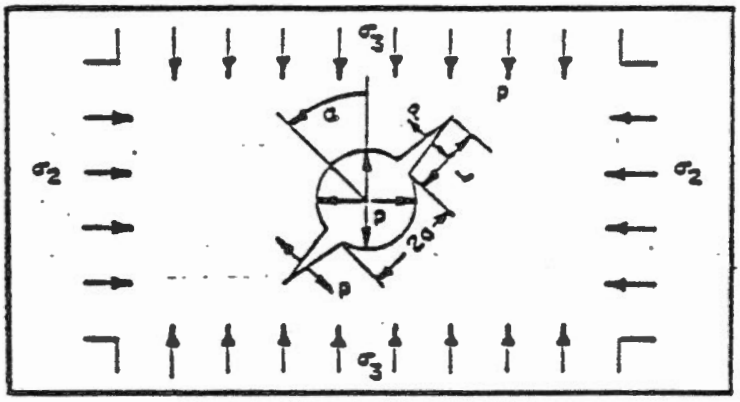

(AFTER ABOU-SAYED ET AL, 1977)

INTERNALLY PRESSURIZED CRACKED BOREHOLE UNDER FAR FIELD STRESS.

FIGURE I

Abou Sayed et al, 1977, consider also a diametrically cracked hole which is internally pressurized (p). This is similar to the situation described earlier (Zoback et al, 1977) except that $K_{II} \neq 0$ in this case.

For this situation:

$$K_I = p\sqrt{L\pi}\, F(L/a) - (\sigma_2 \cos^2\alpha + \sigma_3 \sin^2\alpha)\, F(L/a)\sqrt{L\pi}$$

$$+ (\sigma_2 \cos 2\alpha - \sigma_3 \cos 2\alpha) \cdot G(L/a)\sqrt{L\pi} \qquad (C\text{-}41)$$

F(L/a), G(L/a) - Tabulated Functions

(after Paris and Sih, 1965)

For a tensile crack: $\alpha = 0$

$$(G(L/a) - F(L/a))\, \sigma_2 = \frac{K_{IC}}{L} - F(L/a)\, P_b + G(L/a)\, \sigma_3 \qquad (C\text{-}42)$$

For a shear crack: $\alpha = \pi/4$

$$\sigma_2 = 2P_b - \frac{2K_{IC}}{F(L/a)\sqrt{\pi L}} - \sigma_3 \qquad (C-43)$$

where

P_b - Breakdown Pressure

K_{IC} - Mode I Fracture Toughness

In the opinion of the authors, this analysis seems a little tenuous since if hydraulic fracturing is the result of a shearing action, K_{II} should not be taken equal to zero. Both stress intensity factors K_I and K_{II} should be evaluated.

If the horizontal primitive stress distribution is $\sigma_2 = \sigma_3$ then:

$$\sigma_2 = \sigma_3 = \sigma = P_b - \frac{K_{IC}}{F(L/a)\sqrt{L\pi}} \qquad (C-44)$$

With certain assumptions (C-44) can be expressed alternatively as:

$$\frac{K_{IC}}{F(L/a)\sqrt{L\pi}} - P_b + \sigma_3 = (\sigma_2-\sigma_3)\left\{ \frac{G(L/a)}{F(L/a)} \cos 2\alpha - \cos^2\alpha \right\} \qquad (C-45)$$

"Since the value of the expression in parentheses on the right hand side of equation (C-45) varies between - 1/2 and 1.5 and is near zero only for a limited range of values of α, it is reasonable to expect that, in general, its order of magnitude is not far from unity. Hence, the difference between σ_2 and σ_3 will be of the same order of magnitude as the value of $\left(\frac{K_{IC}}{F(L/a)\sqrt{L\pi}} - P_b + \sigma_3 \right)$.

The last expression contains quantities that either can be measured or evaluated during the field and lab experiments associated with mini-hydrofracturing. More precisely it involves the measurement

of the breakdown pressure, P_b, the shut in pressure $P_s = \sigma_3$, the fracture toughness K_{IC} and an estimate of the length of the pre-existing natural cracks in the formation."

Abou Sayed et al, 1977.

For an initial crack of length L intersecting the borehole and lying normal to the minimum in-situ stress:

$$\sigma_2 = \frac{K_{IC}}{\sqrt{\pi L}\,(G-F)} - \frac{F}{(G-F)} P_b + \frac{G}{G-F}\sigma_3 \qquad (C\text{-}46)$$

G,F – Evaulated for a particular value of L/a

If K_{IC} is found in the laboratory to be:

$$K_{IC} = \sqrt{\pi L_o}\, P_i \dot{F}\,(L_o/a_o) \qquad (C\text{-}47)$$

where:

L_o – length of the crack intersecting the inner wall of a burst sample.

a_o – inner radius of burst sample.

$\dot{F}$ – for laboratory sample

$$\therefore \sigma_2 = P_i \frac{\dot{F}(L_o/a_o)}{(G-F)}\sqrt{\frac{L_o}{L}} - \frac{F}{(G-F)} P_b + \frac{G}{(G-F)} P_s \qquad (C\text{-}48)$$

For L/a and L_o/a_o small, $G \approx 1.5\ F$, giving

$$\sigma_2 \approx 3P_s - 2\,(P_b - P_i\sqrt{\frac{L_o}{L}}) \qquad (C\text{-}49)$$

Abou Sayed et al (1977) state that using Haimson's analysis over-estimates σ_2 :

$$\sigma_2^H - \sigma_2^B \approx (P_b - P_i) \qquad \text{(C-50)}$$

where

σ_2^H – estimated from Haimson's prediction

σ_2^B – estimated by Abou Sayed et al

P_b – breakdown pressure

P_i – hollow cylinder burst pressure

(C.9) ADDITIONAL APPROACHES

Advani et al, 1973, discussed analytical, experimental, and numerical approaches to modelling pressurized fractures.

Analytical Considerations

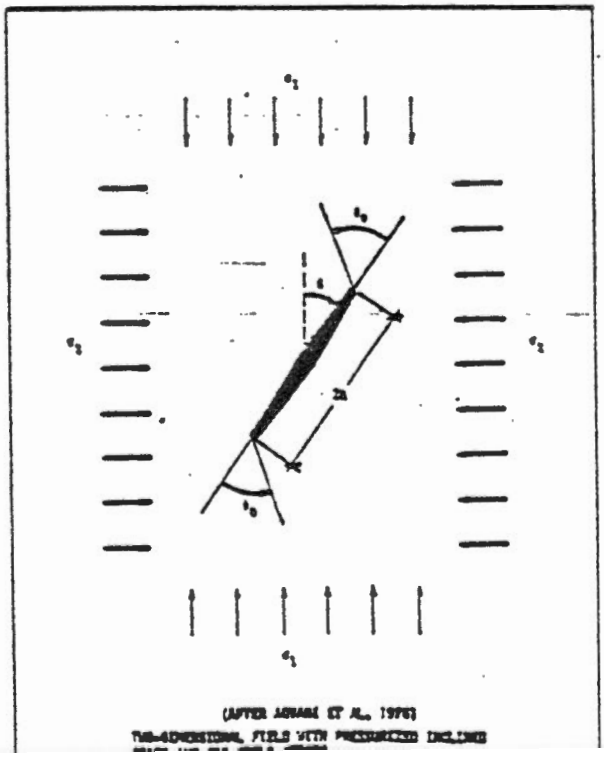

FIGURE J

Figure J shows the idealized model used in the analytical predictions. For this:

$$\left.\begin{aligned} k_I &= \frac{K_I}{\sqrt{\pi}} = (p + \sigma_1 \sin^2\beta + \sigma_2 \cos^2\beta)\sqrt{a} \\ k_{II} &= \frac{K_{II}}{\sqrt{\pi}} = (\sigma_1 - \sigma_2)\sin\beta\cos\beta\sqrt{a} \end{aligned}\right\} \qquad (C\text{-}51)$$

$$k_{II} = 0$$

The stationary angular derivative of the strain energy density is:

$$\frac{dS}{d\theta} = 0 = \frac{a(1+\nu)}{8E}\left\{ (p + \sigma_1\sin^2\beta + \sigma_2\cos^2\beta)^2 \sin\theta\,(2\cos\theta + 4\nu - 2)\right.$$

$$+ 4(p+\sigma_1\sin^2\beta+\sigma_2\cos^2\beta)\sin\beta\cos\beta(\sigma_1-\sigma_2)\,(\cos 2\theta - (1-2\nu)\cos\theta) \qquad (C\text{-}$$

$$\left. + (\sigma_1-\sigma_2)\cdot\sin^2\beta\cos^2\beta(2-4\nu-6\cos\theta)\cdot\sin\theta\right\}$$

For stable crack growth $\frac{d^2S}{d\theta^2} \geq 0$. The critical strain energy density can be found from

$$S_c = \frac{(1+\nu)\,(1-2\nu)\,K_{IC}^2}{2E} \qquad (C\text{-}53)$$

where

ν - Poisson's Ratio

K_{IC} - Critical Mode I stress intensity factor

E - Young's Modulus

As a consequence, the angle of additional incremental crack propagation can be predicted.

Figures K and L summarize the analytical findings.

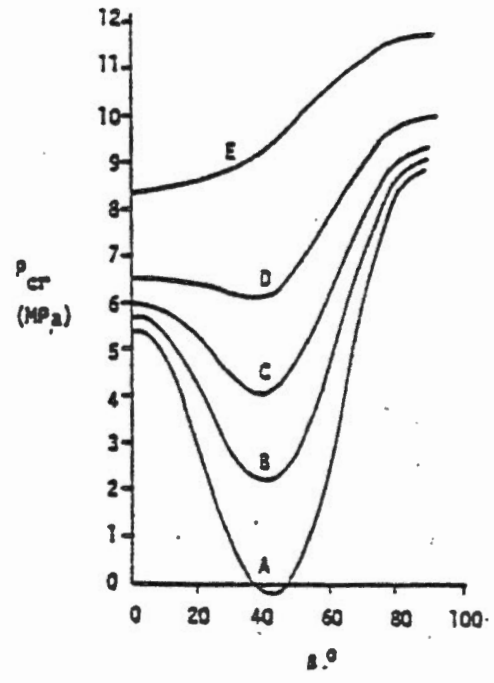

(AFTER ADVANI ET AL, 1976)

$P_{CRITICAL}$ VERSUS INCLINATION β FOR DIFFERENT (AFTER DANESHY, 1973)

FIGURE K

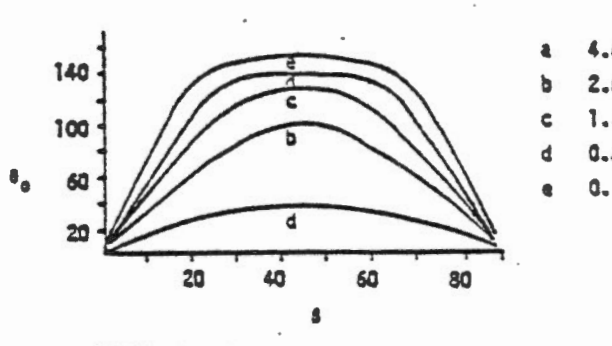

(AFTER ADVANI ET AL, 1976)

FRACTURE EXTENSION ORIENTATION θ_0 VERSUS INITIAL CRACK INCLINATION β FOR DIFFERENT CRACK LENGTHS a_1

FIGURE L